2021

Advance Metallic Reinforcement of Vat Photo Polymerized Parts

Scott Zinn

University of North Florida, n00661846@unf.edu

"Advance Metallic Reinforcement of Vat Photo Polymerized Parts"

By

Scott J. Zinn

A thesis submitted to the School of Engineering

in partial fulfillment of the requirements for the degree of

Master of Science in Mechanical Engineering

University of North Florida

COLLEGE OF COMPUTING, ENGINEERING, and CONSTRUCTION

April 2021

This work is dedicated to:

Dr. Stagon *and* *Dr. Schonning*, *for allowing me a chance to prove myself when others*

would not.

&

Stormy Gaenicke, Amanda Jones, and Rebecca Crosby, *for always being there and*

believing in my abilities even when my own belief began to faulter.

- Thank you

Scott J. Zinn

Table of Contents

4

5

List of Figures

Abstract

The metallization or metallic reinforcement of polymer parts has been widely used in industry for several decades. Polymer parts are classically metallized for aesthetics, chemical and thermal resistance, electrical conductivity, and mechanical strength. Metallization has been shown to increase strength of polymer parts when compared to the strength of the bulk material without metallization. Additive manufacturing (AM) techniques that have emerged in the last few decades produce parts with different surface features and chemistry than the typical polymer part produced through injection molding. AM parts are typically weaker than traditionally manufactured parts from the same material due to intrinsic details and layer interaction. Like their traditionally manufactured counterparts, AM parts will greatly benefit from metallization, but the traditional processes of metallization do not transfer to AM parts due to surface chemistry differences. This work aims to develop processing modalities for the metallization of 3D printed polymer parts from vat polymerization methods.

The metallic reinforcement process is done through sequential deposition of a thick structural nickel plating applied to a conductive physical vapor deposition (PVD) strike layer of nickel that is deposited directly onto the surface of 3d printed cyanate ester polymer base. The resulting structure is a metal-polymer sandwich composition. The overall stress transfer that the composite can experience is dependent on the adhesion strength of the two interface layers (PVD strike to Cyanate Ester, and Nickel Plating to PVD Strike). The performance of the sandwich composite structures are strongly dependent on the adhesion between both of these interfaces, and prior work by Bray et al. in 2019 demonstrated a method of optimizing the adhesion of the PVD strike to the polymer part. However, the presented processing maximized adhesion strength of the Cyanate ester to the PVD strike but came at the reduction of the nickel to PVD strike

interface strength, as the mechanics that increased the sputtered film's adhesion also blocked the mechanics that allowed the Nickel plating to adhere.

This work first explores the mechanisms of adhesion of the PVD strike to the polymer part and uncovers two new phenomena associated with the cyanate ester material that had been previously unknown. The two mechanisms are determined to be advantageous to the strength of the core cyanate ester part but extremely detrimental to the adhesion of the Ni electroplated layer to the PVD strike. The core action of the mechanism is through the percolation and egress of uncured monomer through the PVD strike, resulting in near encapsulation and strong adhesion of the PVD strike to the part but metallic bonding between the PVD strike and the electroplated Ni. After presenting this new understanding, the author concludes with the proposal of an evidence-based processing method for the successful metallization of the cyanate ester parts.

Chapter 1: Motivation and Introduction

1.1 Motivation

Metallization of polymers has become ubiquitous in modern industry. From components in automobile interiors to household appliances, we interact with metallized polymer parts every day in our modern lives. Metallization is a process through which metallic layers, with thicknesses ranging from nanometers to millimeters, is additively deposited onto the surface of non-metallic parts. Polymers are metallized for a variety of reasons, including aesthetic appearance, mechanical strength enhancement, and chemical resistance. y and chemical termination and have been successfully metallized using low complexity processes for more than 50 years. Modern industry is rapidly moving towards using three-dimensional printing (3D printing) as a manufacturing method of polymeric parts [1, 2, 3]. Digital Light Projection (DLP) 3D printing is a method where polymers are photocured into shape, often with subsequent thermal curing [4]. DLP 3D printing produces substantially different surfaces from molded or cast polymer parts, and the metallization of these surfaces has not been sufficiently explored. Motivated by a potential end-use case proposed by Johnson and Johnson 3D Printing Center of Excellence, this work investigates the metallization of SLA 3D printed polymer parts for encapsulation and mechanical reinforcement purposes.

Adhesion and interface interactions are fundamental to the mechanical performance of metallized 3D printed polymers. The ideal metallic reinforcement of a structural polymer is strongly adhered to the polymer surface and has a homogeneous cross-section with conformal coverage of all part surfaces. Conventional polymeric metallization processes rely on the use of electroless, or autocatalytic, plating steps which generate a conductive "strike" layer on the part with strong

adhesion. These classical methods cannot be used on SLA parts due to a homogeneous microstructure and chemical composition. After the deposition of the strike, electrodeposition of thicker layers of metals, most often copper and Ni, is then performed to create structural reinforcement. Classical thermoplastic materials, like ABS, are composed of heterogeneous microstructure, which presents an opportunity for preferential etching to improve mechanical interlocking and surface adhesion. Further, due to the nature of the etchants and the propensity of DLP 3D printed parts for uptake of solutions, the classical etching practices are not applicable to this modern study. Instead, the use of dry methods, such as plasma etching and physical vapor deposition of the strike layer, have been pursued by this group.

Adhesion and interface engineering of metallized 3D printed SLA parts is a two-part problem, consisting of the understanding and optimization of adhesion at two interfaces. The first interface is the region between the polymeric part and the vapor deposited strike. This interface is challenging due to the chemical termination of the SLA 3D printed part surface, as well as the intrinsically smooth morphology of the surface. Mechanical and chemical adhesion mechanisms must be explored to optimize the adhesion at this interface. The second interface is the interface between the vapor deposited strike and the thicker electroplated structural layer. This interface relies on the strike layer to encapsulate the polymer part and prevent any percolation of uncured monomer from the interior to provide metallic bonds at the second interface with adequate adhesive strength.

This work focuses on the development and investigation of scalable and economically feasible metallization processes for SLA 3D printed parts. Development of effective processes will allow for the overall expansion of SLA 3D printed parts into more applications, including those in the medical sector, and will lead to modern goals such as patient-specific geometry and lightweight, recyclable medical instruments.

1.2 Project Overview

The goal of this project is to strengthen and encase additively manufactured polymer parts Figure 1, which are 3D printed using the Digital Light Projection method of additive manufacturing. Mechanical reinforcement is sought to be achieved through electroplating Nickle (Ni) on to the part until a thickness on the order of 50 microns is reached. The Ni encasement has been shown to increase flexural modulus and potentially increase the ultimate rupture strength of the resulting composite part [3, 5]. To make the polymer parts conductive, the process of Physical Vapor Deposition (PVD) was used to coat the surfaces with a thin Ni layer. The PVD process was designed in the first part of the project, led by Ms. Olivia Bray [6]. This first interface presented a significant challenge for adhesion due to intrinsically low surface area and low surface energy of the cured DLP 3D printed part. Early results indicated that, while it was possible to form the strike layer via PVD with strong adhesion, the adhesion of the structural electroplated layer was poor. The initial investigation led to the belief that high intrinsic stress in the electrodeposited films was the cause of poor adhesion. However, the work done in this project demonstrates that the strike is actually compromised by the percolation of uncured monomer material through the strike. While the surface of the strike remains conductive enough to initiate electrodeposition, the interface is littered with polymeric contamination that results in early delamination and the prevention of forming a metallic bond. This work details the investigation into process parameters to first try to avoid the egress of monomer through the strike, which has shown to be increasingly difficult while still providing adequate adhesion to the part. In the end, an alternative method is proposed to generate a viable process path for metallizing the parts with high success.
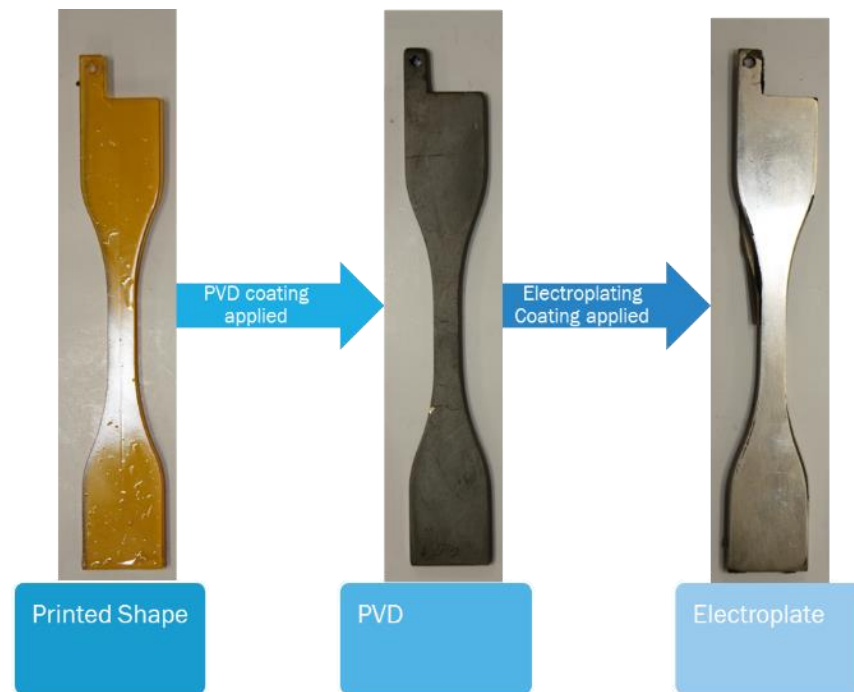
Figure 1 Overview of Project Goal

This project was a culmination of two research theses that involved the optimization of adhesion strength at the interface layer of two different coatings applied to the same base part. A Ni PVD coating applied to a base material of AM cyanate ester was presented in the first thesis undertaken by Oliva Bray from 2018 to 2020 [6]. The adhesion being optimized in the first study was the PVD layer, less than 1 micron in thickness, to the additively manufactured polymer. An electroplated Ni coating was then applied to the PVD sputtered coating, the optimization of which was the initial goal of this project. The adhesion of the electroplated Ni, or e-plated Ni to the PVD-sputtered-Ni was the adhesion in question. The PVD would allow the polymer part to become conductive, which in turn allowed the part to then be electroplated. This would increase the overall strength of the part.

The strength of the coated parts relies on the adhesion of the thick structural layer, through the strike, to the substrate as well as the mechanical properties of the thick layer and the strike. Most of the coated part's mechanical strength derives from the thick e-plated Ni, which has

significantly higher stiffness than the substrate. Increasing the strength at the interface layers would allow the stress to dissipate through more material allowing for an even higher material strength. The interface of the PVD to electroplate forms metallic bonds with one another while the PVD to cyanate ester base could only adhere through imbedding in the material and mechanical interlocking. This would make the PVD to Cyanate Ester (CE) part the limiting factor. The PVD to CE part interface strength was weak enough that the intrinsic stresses generated during the electroplating film formation could delaminate the PVD from the cyanate ester part shown in Figure 2.

Figure 2 PVD surface and Delamination example

The initial process of metallically encasing a CE parts had issues where delamination commonly occurred during electroplating. The film stress generated during film growth is hypothesized be strong enough to delaminate the PVD coating from the CE base part. This process involved CE parts being printed, Cured, PVD (sputtered), then Plated or the CPP process. For this process, the dominating factor that causes delamination, intrinsic film stress generation, could be mitigated to a limited extend by reducing plating factors such as plating rate and temperature. The mitigation was mild though and only delayed the delamination, as it could still occur months later. Ms. Olivia Bray's project found the process PVD (sputtered), cure, then

plate or PCP process, the sputtered PVD layer is strengthen through. In this project, it was discovered that the strengthening of the PVD layer to CE base part, or optimization of interface one, had the unintended effect of weaking the electroplating to PVD adhesion strength, therefore weakening interface two.

Further, in this project it was determined that how and when a part was cleaned prior to sputtering would affect the CE surface layer's ability to maintain a roughness after curing and potentially promoted the percolation of uncured monomer through the PVD layer after sputtering. Leftover resin was observed to fill in microscopic crevasses prior to sputtering, reducing the roughness of the surface and in turn the ability of the PVD interface to remain attached during intrinsic stress generation. After Sputtering, the percolation of monomer was observed to progress, creating an organic fouling layer on the surface of the strike leading to adhesion failure and poor e-plating performance. These results indicated that the overall Electroplate to PVD and PVD to CE base adhesion are optimized when residual polymer percolation is minimized, and the work of the first phase of this project proved to be non-feasible.

The expected outcome of this project is the development of process-structure-property understanding for the metallization of 3D printed multi-step vat photopolymerized parts through sequential treatment, PVD strike, curing, then e-plating Ni. Two requirements must be met to utilize this new method of manufacture safely and effectively: reinforcing of the 3d printed parts, and a characterization of the new materials manufacture and behavior.

1.3 3D printing technology

In the field of additive manufacturing the same manufacturing process can be described using different names depending on the field the manufacturing occurs such as industry,

commercially academia, etc. In the case of this project, the additive manufacturing method used in this project is commonly called in industry and commercially Digital Light Projection (DLP). Though the Carbon© 3D printer employs a patented process called Digital Light Synthesis (DLS) technology, the process outlines that DLP is used in as the polymerization catalyst [5] . Officially, this process method is described by ASTM as a multi-step process that utilizes vat photopolymerization [7]. Though the process and patented names may describe the manufacturing differ depending on field, it is important to know the hierarchy of the technology for future application.

1.3.1 CLIP DLS DLP 3D Printing

In broad terms, CLIP DLS is a multi-step process of vat photopolymerization with subsequent thermal curing to generate a polymeric 3D printed part. 3D printing is a form of additive manufacturing where material is added to create the desired shape of a part. ASTM defines 3D printing as "(the) process of joining materials to make parts from 3D model data, usually layer upon layer…" [7]. In the case of DLP each layer is created through photopolymerization caused by 405nm wavelength light hardening of the resin, this is generated by a photochemical process where a form of light causes monomers to link together to form chains [8].Once the chains form a three dimensional shape, it becomes a voxel, which is the smallest three dimensional shape a printer can create- It can be thought of as a three dimensional pixel. The resolution of the voxels created during the photopolymerization process where the resin is hardened is dependent on the curing light source type and spot size. Carbon© DLS method employs DLP as a catalyst but incorporates different steps to create the final part and continuous liquid interface printing (CLIP) as opposed to typical layering.

Although this project requires the use of DLS 3D printing by the sponsor, there are some obvious benefits of the technology which make it preferable to other 3D printing technologies for many applications. 3D printing done with the DLS DPL process can produce highly toleranced and dimensionally accurate prints. DLP is considered one of the more precise and accurate forms of 3D printing due to the consistent material particle size. This allows the printer to make and outline of the part more closely to the actual shape and can capture fine details. As DLS is a form of 3D printing, it can create parts with designs that traditional forms of manufacturing cannot, opening new avenues of complex design possibilities that do not require the use of advanced CNC or machining methods with lower costs. Additionally, parts generated through CLIP 3D printing are fully dense and do not suffer from layer line defects or layer-to-layer binding, as prevalent in other forms of 3D printing like material extrusion (ME) or selective laser sintering (SLS).

Unlike other forms of DLP or SLA 3D printing, Carbon© uses a unique process to optimize resolution and maximize print speed. Where DLP process requires that bed stage be lifted after every layer is cured to allow fresh resin to fill in the space and be cured, Carbon© uses oxygen that permeates the resin to create what they call a "dead zone" which removes the need for lifting at each layer [5]. This allows for a continuous movement and a faster print time overall, but at the cost that most resins require parts be thermally cured subsequent to printing. This is the case for CE which is the primary resin used for the base materials in this project. CE is chosen for the high mechanical strength and extremely high heat deflection temperature when compared to other polymeric materials that are readily 3D printed.

1.3.2 Cyanate Ester

The CE is the resin used in this project as required by Johnson and Johnson. An additive manufacturing version of the CE developed by Carbon 3D resin was used. The resin is part of the multi-step photopolymerization additive manufacturing process and made up all the 3D printed base polymer parts being plated in metal. CE is a multistep curing resin, which requires more than one form of curing to reach optimal mechanical properties. During printing, the Carbon 3D© printer forms the CE into its desired shape, Figure 3, by photocuring the liquid resin of the polymer using a DLP manufacturing style developed by Carbon© called DLS. Once the part has finished curing, it is cleaned and then cured thermally using a manufacture specified bake cycle. Bake cycles can be unique to the polymer being used. Thermal curing is the last step in the curing process, and once it is completed, the part has reached its optimum material properties. Both processes must be done, or complete polymerization of the ester will not occur. It is particularly noted here that the chemical termination of the parts prior to curing is dominated by uncured CE monomer chains, which have been loosely cross-linked through grafted photopolymer functional groups. The unique nature of this material makes it entirely different from other materials that have been classically metallized in the literature and industry.

Figure 3 Cyanate ester part on bed plate [17]

The thermal curing takes place separately from the 3D printing system in a high-temperature oven over a long period of time, usually overnight. The slow thermal curing of CE parts is done due to the sensitivities that CE has to moisture in ambient environments. If CE were to be rapidly cured or cured without dissipating the absorbed moisture, blistering would occur [9]. In addition, "cyanate ester resins are extremely susceptible to hydrolysis during storage and/or cure. A small degree of absorbed moisture can cause hydrolysis of the cyanate monomer and prevent the primary crosslinking reaction of the network" [9]. If CE parts are not fully cured during cleaning, the resin's final polymerization will be disrupted, creating permanent damage to the part. Additionally, in this investigation, we examine the effects of various cleaning agents on the surfaces of the uncured parts to determine if the adhesion of the strike-part interface can be maintained without compromising the strike-e-plate interface through monomer percolation. Although Carbon® has a recommended cleaning regimen for the parts, the additional investigation was performed to examine if other common chemical solvents could generate a surface with a more stable monomer profile to prevent or limit percolation of the polymer through the strike.

Though there are many processes and chemicals the un-cured resin is sensitive to, once the polymerization is finalized, the polymer boasts a high chemical and heat resistance and stronger strength. This would make it ideal for plating for medical environments due to autoclave procedures with are the primary method of sterilization in hospitals. When using the Carbon® CE resin part, it was observed that intrinsic defect would constantly occur on the top surface of prints, as shown in Figure 4. These defects take the form of fissures that are on average 30 microns deep into the surface. As they are cause on all parts from the printer and not in the cast resin parts, it is assumed to be caused by the Carbon® printing process.
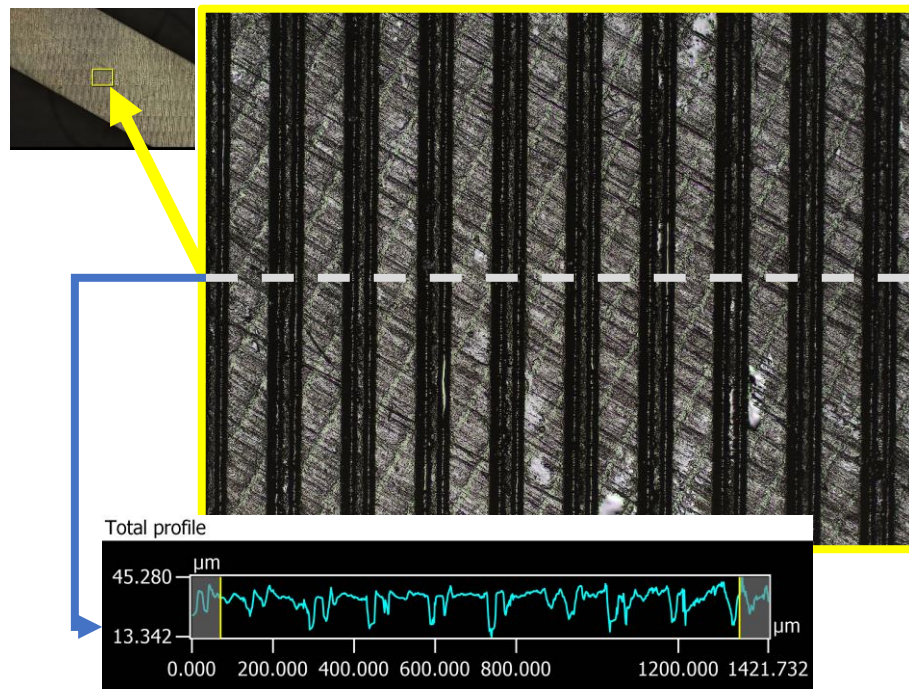
Figure 4 Surface scan of top surface defect of cyanate ester printed parts.

1.4 Physical Vapor Deposition

Physical vapor deposition or (PVD) is a type of vacuum metallization coating technology that produces high purity coatings by transferring a target material, broken down to a molecular vapor. The resulting films are conformal to the part due to the relatively low vacuum level utilized in sputtering, which is on the order of 10^{-3} Torr. In sputtering, an inert gas is flowed at a controlled rate into an evacuated chamber. A large electrical potential, from several hundred to several thousand volts, is then applied between the target material and the vacuum chamber walls and a plasma is generated. The plasma is then attracted towards the target with high kinetic energy due to strong magnets that are placed behind the target. The voltage applied in sputtering is either a constant direct current or a RF current. Direct current voltage is generally used for pure metals while RF sputtering is generally reserved for non-conductive substrate materials. In this work, Ni is used as the strike material, and is also magnetic. Due to the magnetic nature of the target, the plasma plume that is formed is quenched by the target material and higher powers are required.

The power required for a 2-inch diameter target is on the order of 50 to 100w. The PVD process avoids the use of pretreatment steps such as chemicals and etchants that solution-based or galvanic coatings require [1] and avoids the application of thermal energy that could warp or deform the polymer substrate. There are many forms of the PVD process, with the most common being sputtering and the primary form used in this project. The sputtering process involves applying a high energy charge across a target material to attract a chain reaction where the target atoms or molecules are cleaved from the target an imbedded into a desired substrate surface through the kinetic energy [10]. Special considerations must be taken to ensure that the target atoms are able to embed with in the substrate and can be cleaved from the target. The sputtering process occurs within a vacuum chamber and under high vacuum. An inert gas, typically Argon, is used to cause the chain reaction which forms a plasma arc when the high energy charge is applied to the target. The process is illustrated below in Figure 5

When applying PVD films, special considerations should be taken to promote the film growth and adhesion to the substrate. Substrate surface morphology, surface chemistry, mechanical properties, surface flaws, out gassing, preferential nucleation sites, and the stability of the surface are crucial factors in promoting this [6, 11]Diminishing the adhesion of the PVD coating diminishes the strength of the part as a whole.

PVD sputtering is used in this project to provide a conductive layer on the surface of the 3D printed CE parts to allow the electroplating process to subsequently occur. The metal using in the PVD Sputtering metallization process was done with the source target of pure Ni. As the electroplating process applies Ni too, the nickel electroplated onto a PVD Ni layer would adhere in the form of metallic bond. This means the sputtered Ni-PVD coating layer is primarily what it allows the electroplated Ni to encase to the CE parts.
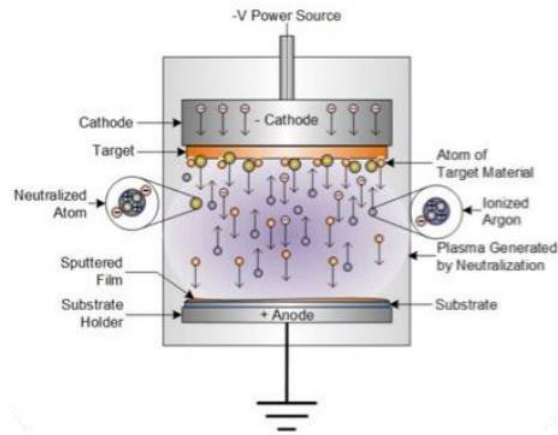
Figure 5 Schematic of the physical vapor deposition (PVD) sputtering process [27]

1.5 Electroplating

Electroplating shown in Figure 6 as the schematic for electroplating, is a process where current induces metal cations from a source metal called an anode, or dissolved in a solution called an electrolyte, to form a layer or coating of these metal cations on an electrode called cathode. The process is driven by electrolysis where an electrical current is used to drive a chemical reaction. The current allows the cathode to gain electrons through reduction and the anode to loss electrons through oxidation. This allows the cations in the solution to bond to the cathode's surface and the anions to dissolve more cations from the anode to replenish the solution and continue the cycle [2]. Electroplating has been performed for more than 100 years and is widely used in industry to produce surface layers on conductive substrates with thicknesses from

several nanometers to several millimeters. The electroplating process is highly sensitive to processing parameters, and different film microstructures and defect densities form depending on the processing conditions.
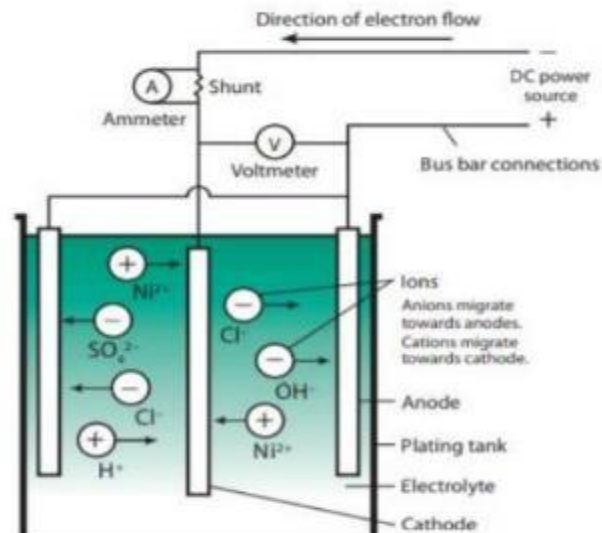
Figure 6 Schematic of the nickel electroplating process [2]

There are two primary reasons to electroplate a part: alter the qualitative and/or quantitative properties. Qualitative is mostly for aesthetic adjustments of features that a part has. A part's luster, color, texture, etc., can all be considered qualitative. Though commonly used in jewelry, these features can have a profound effect on the ergonomics of a part. Quantitative adjustments of features include strength, wear, weight, etc., and are commonly adjusted to meet design strength requirements. All these affect functionalities of a part and most electroplated parts are mixture of qualitative and quantitative requirements more easily met through electroplating.

For the case set forth by the sponsor, the design requires a coating that has a low luster, a plating thickness of 50 microns, and the ability to fail at a higher ultimate stress than the unreinforced group. While the strength requirement is purely a sponsor set goal, a lower luster is desired by the surgeons as it prevents the part from reflecting too much light back during use.

Too high of a luster would make using the part difficult due to the glare it would make. The material used to plate the PVD CE component must be able to maintain high yield stress, to do this the bond between the PVD Ni must be strong making Ni an ideal plating material.

The material used to electroplate the CE substrate was selected to be Ni. Ni has a high modulus of elasticity and ultimate strength. Ni also normally plates with a dull luster and would require the use of brighteners to achieve a higher luster, making it an ideal material for this application. As these brighteners can reduce the strength of the plated part brighteners would not serve any use [2].. The Ni to Ni layering that occurs between the PVD layer and the electroplated surface allows for the Ni to form strong metallic bonds making the weakest point the PVD to SLA interface. Through electroplating with Ni, the CE should be able to achieve the strength levels required to meet the bending stress limit of at first 60 MPa, but preliminary results have revealed other issues.

1.5.1 Process Parameters

In this work used a sulphamate Ni plating solution commonly in industrial applications for thick Ni layers with high mechanical strength and low luster. During the electroplating process, several process parameters can influence the buildup of residual stress within the platting layer. Manufacturers commonly sight variables such as temperature, current density, agitation, pH levels, and filtration as playing parts in controlling the buildup of residual stresses in Ni plated parts [2] [12] [13].

Two process parameters that have a large effect in mitigating stress build up are temperature and current density. Temperature alters the resistivity of the plating solution, and while in the range of 30- 60 C, a higher temperature plating enhances the relaxation of the plated Ni atoms, thus leading to a lower stress in the films. To high of a temperature precipitates the

electrolyte damaging the solution [14]. The elastic modulus of films can be affected but the scatter is often large when in the 30- 60 range making them statically similar on only truly diminishing once outside of the range.

Additionally, pH is a process parameter but going outside of the range 3.5-4.5 only diminishes plating results [2] [15]. Pictured in Figure 7 are to bars plated with the same metal but different lusters. This happened because the pH is outside of the recommended range and hydrogen and impurities begin to increase in density with the metal. Metals may participate out of solution if the hydrogen levels are off and More basic pH can neutralize the sulphamate.

Figure 7 Specimen bars plated at different pH levels, left 5.5, right 3.5

Agitation of the plating solution during plating is also a critical factor in producing films with high strength and uniformity and low stress [3]. Agitation of the part during plating removes gas bubbles that form as a reaction from the electroplating process [14, 15]. If these bubbles are not mechanically removed the plating will become pitted in that area due to the gas pockets preventing the plating solution from contacting the substrate. This also helps with better circulating the plating solution which helps with the cleaning or polishing of the solution during processing through consentient filtering and assuring a consistent ionic load to the metallic surface.

Impurities from the environment, anode and even the specimen being plated can contaminate the solution over time diminishing the quality of the plated layer. In the cause of Ni Sulphonate bath, the pH is very acidic and corrosive. industry recommends polypropylene based filters to strain the contaminates and the use of carbon media to polish the solution even further [2].

A method was developed followed densities to mimic what was found in other research papers. This experiment was never able to be completed due to the inability to fully encase the CE parts easily, though encased parts were tested. The test results from the parts were later removed due to concerns that the cleaner used may have altered the chemical makeup of the uncured CE parts. This concern stemmed from that issue that the cleaner would craze and rip into bed layer artifacts on the surface that would discolor the Ni PVD layer and prevent Ni from electroplating. This led to abandoning testing the current density and temperature and testing surface prep processes This is because specimens would not plate consistently and the mechanism that caused this was unknown. Making experimentally determining an optimized film stress through the factors of C.D. and Temperature optimization too difficult with a base plating film not being grown.

1.6 The PCP Process

Mentioned prior the PCP process stands for PVD, Cure, Plate. This is the process developed where the adhesion strength of the interface surfaces of the PVD coating and CE were optimized [6]. This process is done when CE, the base polymer has a PVD coating applied prior to thermal curing, then plated after thermally curing. The transition that occurs during the thermal

curing process helps the PVD layer adhere to the surface more but come at the cost of extreme sensitivities to surface cleaning and prep [6].

Surface prep, such as solvent cleaning, mechanical abrasion, and chemical exposure, is critical for the success of the PCP process, and PVD coating in general. Surface chemistry, morphology, outgassing, and surface instability are intensified in the PCP process and are key factors in the growth and adhesion of the PVD film [16]. Lax control of these factors leads to contamination or disruption of the PVD film and ultimately causes the adhesion to diminish at the PVD and CE interface.

1.7 Intrinsic Stresses

Intrinsic stresses are stresses that occur within material and are generated through the formation of that material. These intrinsic stresses can usually be referred to as residual stress. Intrinsic stresses form naturally during deposition, and include grain growth, defect annihilation, phase transitions, capillary, interstitial and island coalesce [17, 11]. Intrinsic stresses can be either desired or undesired depending on the overall stress directionality and magnitude. Here, directionality relates to tension or compression, with compression being more beneficial than tension on an encased part. However, if the magnitude of the stress is large enough, regardless of directionality, the stress can cause the material to fail or in the case of this project delaminate from the strike layer. During a loading event, the resultant force being applied will combined with the intrinsic stresses the film is generated during growth and can either increase or decrease the load applied to cause failure.

It is thought that the bending stress that the 3-point bend test applies to the test specimens combines with the intrinsic stresses created during electroplating resulting in a greater resultant

stress than the one being applied. To reach the design requirement of yield stress of 60 MPa experimentation were to be conducted to determine the relation of residual stress to yield stress. Understanding the relation of how residual stresses affect yield stress allows for a more coherent optimization of the manufacturing process overall. This means that the understanding what factors affect the buildup and what are the main modes of residual stress.

1.8 Measurement of Intrinsic Stress

The bent strip test shown in Figure 8 measures the deflection of a thin strip of material resembling a tuning for with two prongs or cantilever beams, that is being electroplated. Each beam is only able to be plated on one side allowing for the measure of tensile and compressive intrinsic stresses built up on each side of the bath during the plating process [15] . This allows the measurement of the intrinsic stress that electroplating can impart onto the PVD film. If the intrinsic

Figure 8 Bent strip test schematic [15]

stresses overcome the adhesion strength, then the PVD film could delaminate form the CE surface.

Chapter 2: Methods Utilized

2.1 Substrate creation

All samples for this study were created using CE 221 resin from material provided by Johnson and Johnson 3D printing center of excellence carbon [18]. The additively manufactured test groups were printed on the proprietary Carbon 3D printer at the most rapid print speed setting with the minimum resolution setting. The cast CE test group samples were made from a sheet cast by pouring the CE resin from the Carbon© cartridge into an aluminum baking tray, as depicted in Figure 9. This tray was then placed into the Carbon© cure machine where it was cured for the standard thermal cycle recommend by Carbon©. Photo curing was not employed due to recommendations from Johnson and Johnson that a photo cure would not be necessary. Additionally, no release agents or chemicals were added to the cast or mold tray. The tray was removed from the cast without causing damage to the cast CE sheet as shown in Figure 9 and Figure 10. It is worth noting that the resin samples that were not photo cured seemed to expand during thermal curing. Test specimens were cut to the ASTM D790 standard specifications using a band saw and milling machine, the sheet was cut using a rotary tool and cutting wheel to avoid damaging the brittle material [19].

Figure 9 Cast Cyanate Ester, in Aluminum Tray
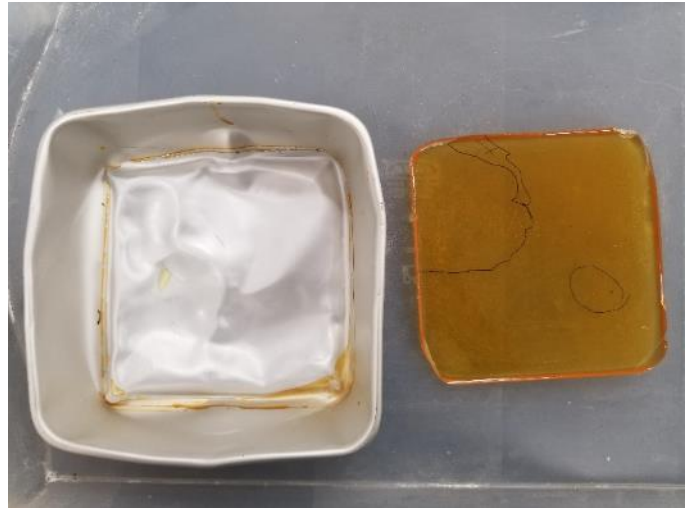
Figure 10 Cast Cyanate Ester, removed from Aluminum Tray.

After the CE cast was created, the 3D printed CE test group samples were manufactured. Manufacturing was done utilizing the Carbon© 3D printer, and STL files from the ASTM D790 test specimen specifications Figure 11. Print orientation for all test samples are depicted in Figure 12. This orientation was chosen due to layer orientation being parallel to load allowing for the theoretical maximum material strength. The groups printed include the printed control and reinforcement samples. The printed control groups were used as a comparison for additional strength that the reinforcement process provides and collect base material values used for later hand model calculations. The results of both printed groups compared to the cast control will help validate the use of the test standard. All sample sets were composed of at least n = 5 samples, with most sample sets being composed of n = 10 samples.

12,7   3,2

60,8
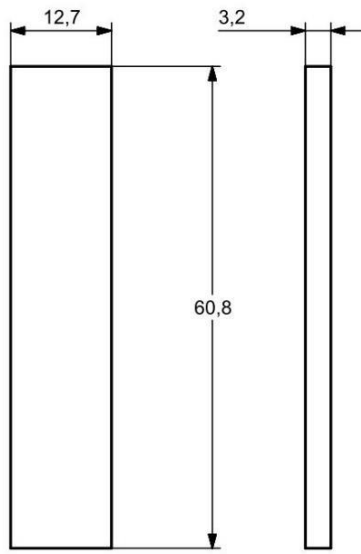
ASTM D-790

Figure 12 ASTM D-790 Specimen Drawing in (mm)

Build Direction
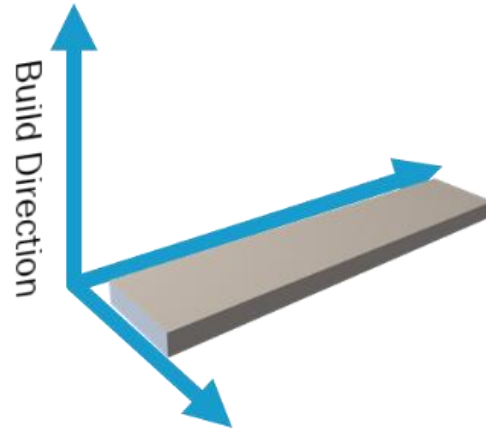
Figure 11 Flat Build Orientation

The CE cast test group was included at the request of the thesis committee and is generally suggested and used by ASTM testing community members. Casting is generally considered to be the traditional manufacturing method for a baseline comparison of polymer printer parts. In this case, it is used as a method of validation for using a non-A.M. specified standard for experiments using AM parts. It is assumed that the cast CE would provide the highest possible stress values when testing due to the cast material being a solid continuous part with a lack of defects. Additively Manufactured parts intrinsically create defects during manufacturing and create parts in a layering process that rely on material strength and layer adhesion for the overall material strength.

2.2 Sample Prep

The process in which a PVD layer is applied before curing required that the parts be cleaned prior to the PVD application. Not doing so would cause massive outgassing in the vacuum chamber which hindered the PVD application, and the PVD that was applied to raw resin could

easily be wiped away. This cleaning process was previously completed by Johnson and Johnson, however, now had to be completed on site. This led to the realization that the cleaning method is hugely paramount as well as how the parts are handled after a PVD layer is applied.

Prior to any application of PVD sputtering, parts were cleaned using the following steps outlined in Table 1 Standard cleaning process for PCP process:

Table 1 Standard cleaning process for PCP process

Step	
1	Wipe surface with chosen Cleaner to remove excess resin.
2	Fully submerge parts in a bath of Cleaner.
3	Agitate using an Ultrasonic cleaner for 100sec or orbital stage for 120rpm for 6min.
4	Remove from bath and rinse or submerge in DI water.
5	Blot Dry.
6	Repeats steps 2-5 once more if needed

Wipes dipped in the cleaner solvent were used to remove the bulk of the resin from the part to extend potency of the bath chemicals. The bath was agitated with the use of an Ultrasonic cleaner or Orbital shaker stage to thoroughly remove surface resin that adhered to the part. This reduced the need for human intervention during the cleaning process which was ideal for this project. Deionized water was used to remove the cleaned resin stuck to the surface, deactivate the cleaner used, and allow for Step 6 to have more effect on resin missed during the initial bath.

2.2.1 Sanding

In order to introduce surface roughness into the specimens, some test groups were wet sanded using 400 grit sandpaper. This occurs in the PCP and CPP process prior to any PVD sputtering.

2.2.2 Hanging and handling

Safety precautions were adhered to by wearing nitrile powder free gloves at all times while handling the specimens in order to limit the disruption of the surface of the coating with oils from the hands as well as to protect against CE's carcinogenic nature. When not being sputtered or plated, specimens remained in a sealed bag within a dark, dry drawer until use. This was to limit the over exposure to light that could over cure the specimens.

It was important that specimens were cured quickly once the PVD coating had been applied. However, the printing schedule of Johnson and Johnson, vacuum chamber process, and the leftover resin protocols limited the ability to manufacture only the needed specimens for a sputtering cycle. Due to photo exposure and moisture exposure, the leftover resin had to be disposed of after each printing job. The maximum amount of time that Carbon recommends for uncured parts waiting to be cured is approximately two hours, which is the same for the usability of the vat resin. The vacuum chamber, though removing the specimens from environmental exposures, still took roughly 5 hours per coating process which each sample group tested need two of. Due to the mentioned constraints, the majority of printed specimens were not able to meet the two-hour window.

During curing, specimens were not specified to be hung or oriented in any particular way, aside from the experiment where curing orientation's effect on the polymer percolation was tested.

2.2.3 Solvents

Four solvents were used when testing the surface prep techniques: Propylene Glycol & Isopropyl Alcohol mix, Isopropyl Alcohol, Denatured Alcohol, And Acetone.

The Propylene Glycol & Isopropyl Alcohol mix was the solvent mixture Carbon recommended cleaning CE parts with Figure 13. The manufacturer recommended cleaning solution is a 50/50 mixture of 99.9% Isopropyl Alcohol and Propylene Glycol for all experiments with the brands depicted in Figure 14 and Figure 15 and. The printed parts are to be wiped thoroughly and cleaned with the mixture using an orbital shaker for 1 minute, then be bolted dry. Though this method was recommended by the manufacturer, it is not commonly used by Johnson and Johnson.

CE 220/221 — V04.00

MAX. TOTAL SOLVENT EXPOSURE TIME: 3 MIN
SOLVENT: 50/50 IPA + PG   BAKE TIME: 12.5 HRS, Program 1 Pattern 1

WASHING
Note I: IPA/PG solvent mixture is more viscous than IPA and does not evaporate as quickly.
1. Remove liquid resin by using the compressed air cabinet, wipes or swabs.
   a. Pay attention to grooves, recesses, and hollow spaces that trap resin.
2. Fill empty container with IPA/PG mixture so that when parts are added they will be about 75% covered.
3. Place parts in IPA/PG and quickly wash on orbital shaker for **1 MIN at setting 2 (120 RPM).**
4. Remove solvent residue from parts by using compressed air cabinet or blotting.
   a. If blotting, gently press lab wipe onto surface of parts to absorb solvent.
   b. Gently wipe solvent from smooth, cosmetically important surfaces.

CURING
1. Place clean parts on non-stick baking tray. Support parts with non-stick foil if needed.
2. Bake parts using **Program 1 Pattern 1.**
   a. Baking process will take **12.5 HOURS.**

Figure 13 Carbon© Recommended Cleaning and Curing Process for C.E

Figure 15 Belle Chemical Brand 99.9% Isopropyl Alcohol

Figure 14 Belle Chemicals Brand Propylene Glycol

The acetone used in this study was the Acetone shown in Figure 16, which was introduced to this study by mistake from one of the J&J personnel. It was suggested that in the place of IPA, which was very scarce at the time, Acetone be used to clean the parts as it would have no effect on the polymer base. Unfortunately, this was not the case as acetone has the ability to exasperate bed layer artifacts and vowel surfaces as shown in Figure 16. Denatured alcohol pictured in Figure 17 was used as form labs, another 3d printing company recommended cleaning parts with this solvent. Denatured alcohol led to parts with mitigated polymer percolation layers but having similar effect to acetone.

Figure 16 Klean Strip Acetone

Figure 17 Denatured Alcohol.

2.2.4 Ultra-sonic bath

The Sper Scientific brand of ultrasonic cleaner pictured in Figure 18 was used for all samples cleaned with the ultrasonic bath which is capable of vibrating at a frequency of 42000Hz. When this happens, the vibration creates bubbles that then caress the surface providing a high caliber of cleaning with minimal effort or abrasive use. Commonly, samples cleaned using the ultrasonic method were placed in a beaker with the desired cleaning solution such that the samples were completely submerged at ambient temperature for 100 secs.

2.2.5 Orbital stage

The Orbital shaker used was the KJ-2018BD orbital shaker Figure 19 loaned from the Johnson and Johnson center of excellence. When cleaning with the orbital stage, the manufacturers recommended method of cleaning was used. The agitation process the manufacture recommended was that the samples be 50% submerged in the cleaner and orbited at a rpm of 120 for 6mins.

Figure 19 Orbital shaker used during study.

Figure 18 Ultrasonic Cleaner

2.3 PVD Method

The PVD method used was copied from Ms. Olivia Bray [6]. This was because Bray's main objective in her research was to develop the method of PVD coating application specifically for this project. The target material used was 99.9% pure Nickel measuring 2 inches in diameter and 0.125 inches thick (Kurt Lesker, Jefferson Hills, Pa., USA). The sputtering gassed used was 99.99% pure Argon gas. The space in the chamber allowed for up to five test specimens to be laid flat and rotated automatically without being knocked off the stage or rubbing against the chamber wall.

The sputtering process was conducted in the vacuum chamber shown in Figure 20. After cleaning and prep. A layer of Ni was applied using magnetron sputtering once the vacuum pressure reached a value less than $9*10^{-5}$ Torr. Each specimen was coated over the course of 30 minutes and then flipped and sputtered again for a total of two sputtering applications per specimen batch. The Ni PVD layer applied to the total surface area was less than 1-micron. After two successful PVD coatings, the specimens would be inspected for coating quality.

Figure 20 Vacuum Chamber

Once parts were fully coated in PVD, a chemical wipe test was employed. A 99.9% IPA wipe was used to wipe each surface of the part, and a Klean Strip brand Acetone wipe was wiped in the top. This was done to confirm little or no PVD was removed by the chemicals. If removal of the PVD occurred to the point at which bare CE was visible, the specimen would undergo another PVD coating application. Acetone was only used on the top because acetone has the ability to rip open the bed layer artifacts present on the bottom layer of the print. All specimens that underwent the chemical wipe test were submerged in water to neutralize the chemical reaction and limit overexposure. Once specimens passed the chemical wipe test, they were given to Johnson & Johnson to undergo the curing cycle overnight and delivered the next morning for plating.

2.4 Electroplating

Once delivered, the cured parts would be electroplated using a Ni sulphamate solution bath set up shown in Figure 21. The electroplating solution used Ni sulphamate was picked for the enhanced mechanical properties and visual properties the sponsor required [2]. To apply a thickness of 50 micron of Ni during plating. the steps outlined in *Table 2 Multi-Current Plating Process* were used. Specimens that had a layer of PVD Ni applied and cured were plated with a seed layer of electroplated Ni at a current density of 0.5 A/dm^2 for 5 mins. This was done to allow for a thin layer of Ni to adhere to the PVD surface and allow for easier dispersal if the current across the surface without the high intrinsic stresses that occur when platin at higher current densities. After the five minutes at 0.5 A/dm^2 the specimen was plated for 5 mins at 1.0 A/dm^2, then inspected for plating quality. Specimens observed to have a spotty plating coverage were removed from the study. After the inspection, the specimens were put back into the bath and plated for 115 mins at 1.0 A/dm^2, then 60 mins at 2.0 A/dm^2 to finish the plating thickness of 50 microns. The current density of 2.0 A/dm^2 was done to allow most of the plating film to generate

with a lower stress than would occur plating at 4.0 A/dm^2 and the final current density 4.0 A/dm^2 was done to reduce the time test specimens took to plate due to the limited time span.

Table 2 Multi-Current Plating Process

Figure 21 Electroplating Bath Setup

Step	Current Density (A/dm^2)	Time (mins)	Overall Thickness (microns)
1	0.5	5	>1
2	1.0	5	2
3	1.0	115	23
4	2.0	60	25
Total	~	~	50

Anodes were constructed using 99.9% pure Ni sheets and titanium wire as depicted in Figure 22 on right. The titanium wire was used to evenly disperse the current across the anode

and would not corrode with in the bath [2]. The titanium wire would be wrapped around the anode in a chain link fence style then be put into Anode bag.

The anode bags, Figure 22 in the middle, were created from polypropylene filter mesh and plastic welder. The polypropylene filter was cut in the rough shape of a bag then had the edges welded together using polypropylene welding filament. The bags were used to trap larger Ni fines and impurities that could the reduce the plating quality of the electrolyte. The quality of the bags and anodes were checked prior to plating by verifying the anode and bag were intact.

The Agitation and filtration system was constructed using a Zoo med canister filter and self-made filter bags with carbon filtration media shown in Figure 23. The agitation came from the filter system's flow output which, for the small size of the bath container, was acceptable and removed most bubbles. Carbon media was used as it was the common practice of industry to have continuous filtration and agitation with a carbon-based filtration system [2]. [14]The filter bags pictured in Figure 23, were made from polypropylene filter mesh as polypropylene would not deteriorate from the solution's corrosive effects. The bags were made by using polypropylene plastic welder to join the edges shut. The carbon media was refreshed every month.

Figure 23 Anode and anode bag set up, (left) Anode in bag, (middle) Anode bag, (right) Anode wrapped in Ti wire.

Figure 22 Filter Pump Head with Carbon Filter attached

A standard 1000ml Borosilicate glass Beaker was used to contain the electroplating solution bath and the dual mounted anodes. This container was chosen over other due to the unreactive nature of the glass and thermal properties. Due to the bath's ideal pH range being between 3.5-4.5, a glass beaker was ideal to resist the corrosive nature and can withstand the temperature levels the electroplating bath's solution needed to operate at.

Temperature was controlled by a Corning hot plate and measured using a thermocouple. Due to the lack of a system controller, the thermocouple needed to be observed to ensure the temperature did not fluctuate outside +- 5 C of the intended temperature range. The operating bath temperature range was decided to be between 30 C-40C the range was chosen due to literature stating temperature below 35 C have no effect and temperatures exceeding 65 C damage the plating solution [2] [14]. When in use, the Hotplate would be turned on to heat the bath to one of the thermal levels. Once the hotplate reached a certain range dependent on the dial setting chosen, it stopped heating up and reached a steady state with no drastic increase of decrease to the output energy. The temperature would then be measured using a thermocouple to confirm if the ideal temperatures were met.

The current applied to the anode was done using a Kuman power source pictured in Figure 24.onstant current mode was chosen with the current output applied to the two anodes altered to fit the desired current density. Current Density measured in A/dm^2 was calculated using Equation 1 Average coating thickness.

Equation 1 Average coating thickness

$$T = 12.294\frac{It}{A}$$

T: Average thickness (μm)

A: the surface area being plated (dm^2)

I is the current through the plating solution in (A)

T: time the current is applied (hours)

12.294: Chemical Coefficient (this assumes 100% cathode efficiency)

The pH level of the solution was measured each time prior to plating, once the plating solution reached a pH greater than 4.5, diluted sulfuric acid was used to lower it [2]. If the pH was too low more solution was added to balance the system, then the solution was agitated and filtered to improve homogeneity. A generic pH meter shown in Figure 25 was used to confirm the pH range did not fall outside of the desired range of 3.5 - 4.5. This was chosen from industry literature as an ideal range for the Ni sulphamate solution [2]. A pH outside this range had the ability to plate more impurities from the bath solution and if the range increased to much participate the Ni ions from the solution [2] [12]. If pH levels reached a range greater than 4.5, diluted sulfuric acid was used to decrease the level and allowed to filter through to meet homogeneity as seen in literature [2].

Figure 25 Generic pH tester
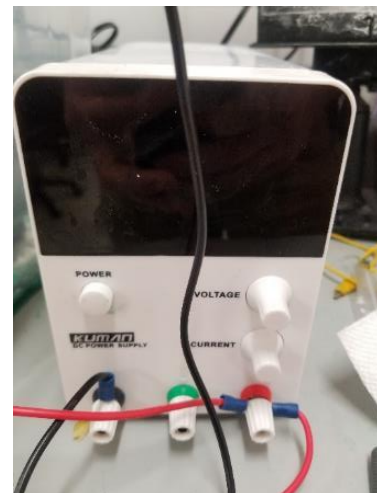
Figure 24 Kuman Variable Power source

2.5 Optical & Laser Microscopy

Optical microscopy is commonly used for the initial examination of surfaces due to the relatively higher ease of use and low cost. Though magnification is limited compared to Scanning electron microscope (SEM), basic fractography and analysis can be completed to gather an overview, possible points of interest, or final determination prior to using a SEM. The model used in this project was the Keyence VHX-7000 Series Digital Microscope pictured in Figure 26. This model uses both visible light in the form of a laser at 405nm wavelength to produce, and optical image accompanied by a surface height map. The microscope was used to gather all surface scans and images seen throughout the paper.

Figure 26 Keyence VHX-7000 Series Digital Microscope [16]

2.6 Fourier Transform Infrared Spectroscopy (FTiR):

Fourier Transformation Infrared Spectroscopy is the standard method of infrared spectroscopy and is used to identify organic or even non-organic materials. This is done through measuring the

absorption of infrared radiation versus the wavelength of the sample [20]. The output is an infrared spectrum that acts as a fingerprint for the sample, with absorption peaks that relate to the vibrational frequency of the bonds in the sample. The samples spectrum can then be used to identify what material is present and the amount. In this project the FTIR was used to establish if polymer was percolating through the PVD strike surface after different solvents and methods were used. One sample from each cleaning group was tested and, in the end, samples exhibited some form of organic material on the surface, leading to the discovery of "Surfactant Layer Generation" or SLG formation.

2.7 Material Test methods

The method of testing used was ASTM D790-17 Standard Test Methods for Flexural Properties of Unreinforced and Reinforced Plastics and Electrical Insulating Materials [19] to determine the maximum flex stress for reinforced polymer parts. The specimen geometry used is depicted in Figure 11. A three-point bend test was used which provides the stresses associated with bending, since the polymer is 3D printed and ASTM do not have any adopted method of three-point bend test of reinforced additively manufactured parts.

The D-790 Type I 3-point bend test was used for all testing, while Procedure A was used for the test groups Cast CE and the Metallically reinforced test groups, Procedure A was used when the Printed control group failed to fracture in the 5% strain limit. The D790 standard [19] was chosen over the C393/C393M [21] method for two reasons: due to the C393 method's test specimen size would not fit within the vacuum chamber during the PVD Process, and the consistent use of the D790 specimen design allowed for easier direct comparison of material properties. All material testing practices followed the guidelines set by D790 testing practices when conducting 3-point bend tests.

2.7.1   Three Point Bend

Three Point bend test setup as depicted in Figure 27 as chosen over four-point bend test to evaluate the material strength at a point rather than the entire loading area that would occur during four-point bending. As the tested parts were 3D printed, the inclusion of defects intrinsic to the additive manufacturing process [22] would be predominantly tested over the strength the provided by the reinforcement. In the end, J&J decided that the three-point bend test would also be more desirable over the four-point bend method, as the strength provided by the reinforcement was more important than the encasement of the CE parts.

Figure 27 Three Point Bend Test Setup

All test samples were tested on a Shimadzu 5kN vertical load frame Figure 27.The force and displacement data were collected from the load frame and used to calculate ultimate stress and strain using the equation provided by ASTM [19].

Equation 2 Flexural Stress (σ_f):

$$\sigma_f = 3PL/2bd^2$$

where:

σ_f = stress in the outer fibers at midpoint, MPa (psi),

P = load at a given point on the load-deflection curve, N (ldf),

L = support span, mm (in.),

b = width of beam tested, mm (in.), and

d = depth of beam tested, mm (in.).

Equation 3 Flexural Strain (ε_f):

$$\varepsilon_f = 6Dd/L^2$$

where:

ε_f = strain in the outer surface, mm/mm (in/in),

D = maximum deflection of the center of the beam, mm (in),

L = support span, mm (in.), and

d = depth, mm (in.) of beam tested

Equation 4 Max Allowable Strain

$$D = rL^2/6d$$

where:

D = midspan deflection, mm (in.),

r = strain, mm/mm (in./in.),

L = support span, mm (in.), and

d = depth of beam, mm (in.)

All sample groups included five specimens that were tested until failure, or the maximum strain of the outer surface had reached 0.05 mm/mm in accordance with the ASTM guideline [19]. Samples that failed at an outer strain greater than 0.05 mm/mm were removed from the test data pool and replaced with qualifying samples until the test group reached five useable test specimens for each group. The load Ultimate Stress and the test groups included CE cast, CE printed, and CE printed and then reinforced.

2.8 Chemical and UV Exposure methods

Johnson & Johnson personnel raised concern that the orientation of how the parts were placed on the curing tray could affect BLC and SLG formations. The theory was that surfaces in contact with the metal bed could over-thermally cure and lead to the creation of the SLG layer and by consequence, BLC formation. Due to limited time but the need to determine a quantitative assessment of the intensity of the BLC and SLG formations as relates to cleaning processes used, both projects were combined.

The polymer percolation formation was believed to be caused by two things: cleaning methods and curing orientation. The testing involved two response factors: solvents and agitation methods or orbital stage, and ultrasonic bath used. The specifications of which are as follows:

- Solvents
  - IPA

- o   IPA + PG

- o   No cleaner

Each solvent was tested using:

- No agitation (wiped with cleaner)

- Agitation without wiping

- Both wiping and agitation.

From the specimens, surface scans were taken at pre cure and post curing. The scans were done on all specimens and included an optical and laser topography scan at 20x with a Keyence microscope to determine the amount to roughness each specimen's surface had pre and post thermal cure.

The test specimen geometry used in the exposure experiments were of a rounded square bar shape depicted in Figure 28. The specimen was purposefully designed to have an attachment spot and have equal surface area on all sides. This was so the effects of the print surface, top, bed, and voxel(side) surfaces could be gauged equally. The specimen was exposed to cleaning chemicals over time while in an ultrasonic bath, while the UV exposures were conducted separate from the chemical exposures study and with a 405nm UV lamp with bot time dependent gradient exposure studies.
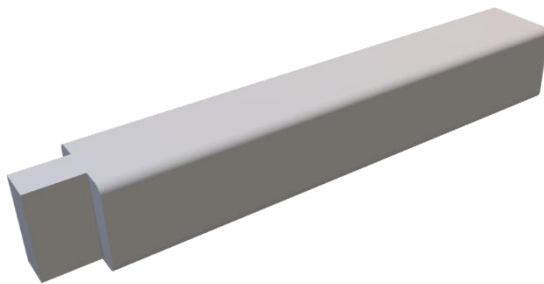
Figure 28 Cleaning specimen design

Chapter 3 Two Interfaces, Two Optimizations

As with most coatings, the most important property related to the performance is the adhesion strength of the additive layer to the substrate. Without adequate adhesion, the coating is prone to delamination, rumpling, cracking, and other failures. Particularly in the case of coatings to increase strength, the adhesion to the substrate is key. An increase in the adhesion strength of the coating substrate's interface creates an increase in the transfer of stress between the substrate and the shell without rigid body translation between the two. In this project, it is essential to create a mechanical framework via coating of the substrate which increases flexural stiffness, increases the ultimate strength at fracture, and provides an encasement or encapsulation to the interior part to prevent the egress of liquids.

Unlike in typical single layer coatings, in this project there are two interface layers. The first interface is the interface between the CE substrate and the PVD strike and the second interface is between the PVD and E-plate. Traditionally, PVD films are plated onto non-metallic substrates and the interface with substrates is dominated by monolayer-to-monolayer, mechanical interlocking, diffusion (alloying), compound, and pseudo-diffusion [16]. Likewise, in this work, the interactions with the polymeric substrate will be dominated by physical bonding and rely on mechanical interlocking for adhesion. In prior work by Bray, the adhesion was seen to be optimized through deposition of the PVD strike onto the uncured CE substrate. In this work, we determine the mechanism through which this adhesion increase is possible and demonstrate the downstream effects on subsequent processes. Alternatively, electroplated films interface primarily through metallic bonds, and secondarily through mechanical interlocking as the substrates that can be electroplated onto, must be conductive and are primarily metals [15] [2]. As stated earlier, the PVD interfaces with the CE through mechanical interlocking, which we observe to be

increased through surface relaxation during curing, and electroplating uses both. Of the adhesions depicted in Figure 29, the Interface 2 (E-plate-PVD), which is expected to form metallic bonds, should naturally be the stronger than Interface 1 (CE-PVD), which is essentially friction and vacuum from the "trapped" gas pockets under the film. In this work, we experimentally determine that the second interface between the PVD strike and the E-plate is significantly compromised by the egress of monomer through the PVD strike during curing and vacuum deposition. The egress is characterized here using optical microscopy and FTIR and is demonstrated to cause increased contact resistance and very poor adhesion between the e-plated layer and the PVD strike.
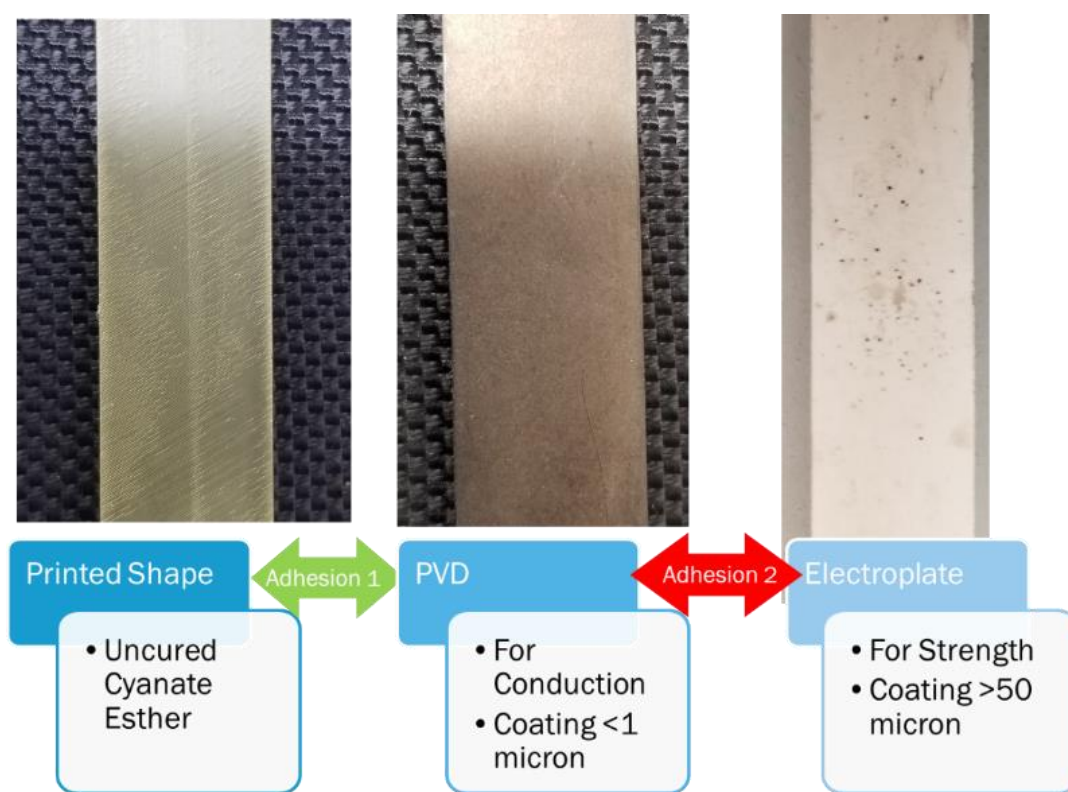
Figure 29 Visual representation of the two interface adhesions

3.1 Interface 1

Interface 1, as shown in Figure 30, is the strength at the interface layer of the PVD to the CE. As there should theoretically be no chemical bonding that occurs with Ni and CE, the adhesion mechanism is mechanical interlocking, that is based on friction and substrate incasement. Unlike the case of thicker films, as the PVD strike is on the order of 100 nm in thickness, as measured in Bray, there is little mechanical strength and almost no encasement factoring into the adhesion. The mechanical interlocking is primarily due to projected surface area, with higher surface areas generating greater lengths for friction and physical bonds to occur. If the adhesion strength of Interface 1 is decreased, the entire structure may be compromised as stress flow will happen non-uniformly from the disconnected external shell to the interior substrate. Although this adhesion was optimized in Bray, we determine the mechanism for this optimization here and again illustrate how the means used to improve the adhesion led to compromised adhesion between the PVD strike and the e-plate.
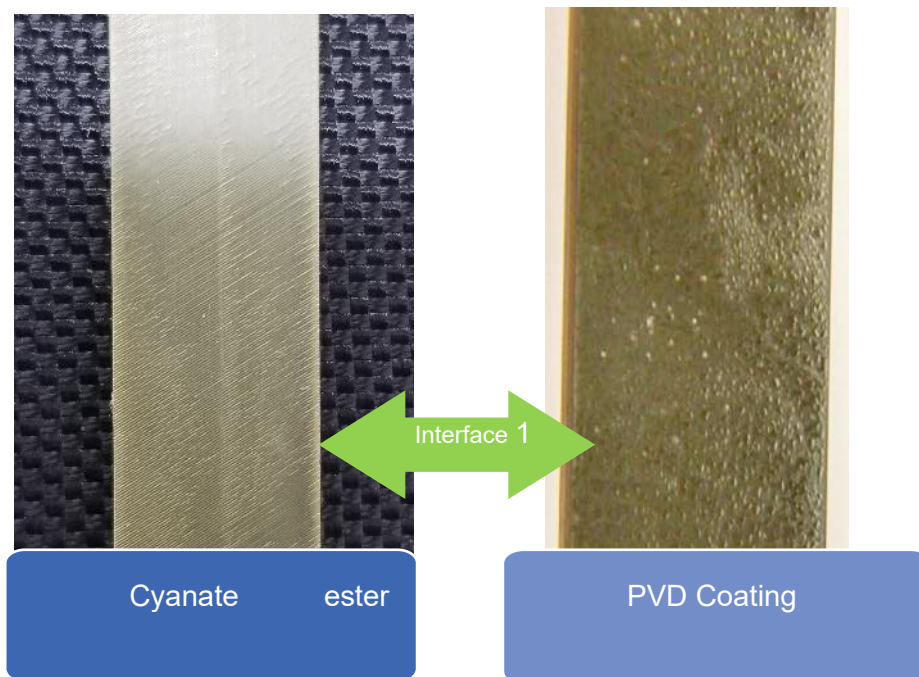
Figure 30 Cyanate ester part (left), PVD-Cured Cyanate ester (right)

In prior studies, initial PVD coatings were applied to the CE after it had been thermally cured in a process shown in Figure 31. This process was notorious for failing during electroplating in the form of delamination failures.
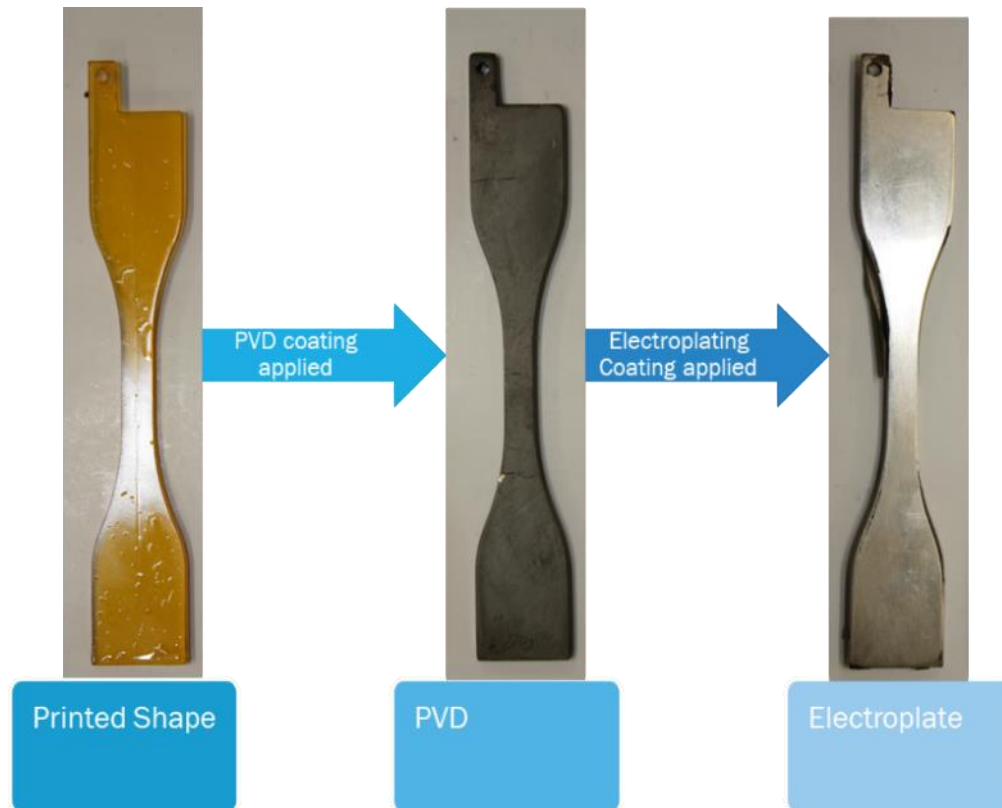
Figure 32 Cure, PVD, and Plate (CPP) process

In this paradigm, the intrinsic stress that develops when growing the electroplate film would overcome Interface 1's strength, causing the film to peel up and curl removing the PVD layer with it. As we will demonstrate later in this work, adhesion is poor due to reduced surface roughness caused by a polymer formation and smooth layer, here called a BLC layer, and the reduced embedded layer depth caused substantial reduction in Interface 1. The failure also emphasizes in how the Interface 2 strength the Ni PVD to Ni electroplate interface is at its maximum as no PVD coating was left on the surface. This is important to note, as failures that occur using the PCP process do not exhibit this same behavior.

Introducing surface roughness back into the surface of the CE would increase the friction and Interface 1's driving mechanics. Commonly, surface roughing for PVD coating is done with acid etching. This would not work in this case, as cured CE is highly resistant to acid etching and has a homogeneous microstructure, and thus was abandoned. Sanding parts prior to PVD showed much promise as parts could be fully encased as shown in Figure 32, but was also abandoned once the PCP process was discovered as the scalability of the PCP process appears superior.

Figure 33 Example of sanded specimen being successfully encased.

The theory behind the PCP process is that instead of introducing surface roughness post cure, the PVD coat was applied to the surface before curing. It was hypothesized that the surface relaxation and monomer mobility during the curing process would likely increase the true surface contact area between the strike and the substrate and increase adhesion strength. This process does indeed maximize the strength of Interface 1, as the more ductile and rough material of the uncured part allowed the PVD layer to mechanical interlock with the surface easier. After which, the PVD would become encased during thermal curing due to percolating polymer formations. This increased the buried interface and kept the original surface roughness of the base part. Additionally, the formation of the polymer layers increased the mechanical interlocking for the

PVD film which led to the maximization of Interface 1. Unfortunately, the maximized Interface 1 strength came at the cost of a minimized Interface 2 strength due to percolating polymer formation layers.

3.2 Interface 2

Interface 2 is the interface illustrated in Figure 33 of the Ni PVD film and the Electroplating film. As previously mentioned, the adhesion mechanics are metallic bonds and surface roughness. The strength of Interface 2 is paramount as the bulk strength of the part comes from the 50 micro-Ni plate. Typically, interface 2 would be the stronger adhesion due to the metallic bonds, but this is not the case due to the blocking/inhibiting of the metallic bond formations and reduced surface roughness caused by percolating polymer formations.

PVD

Adhesion 2

Electroplate

- For Conduction
- Coating <1 micron

- For Strength
- Coating >50 micron
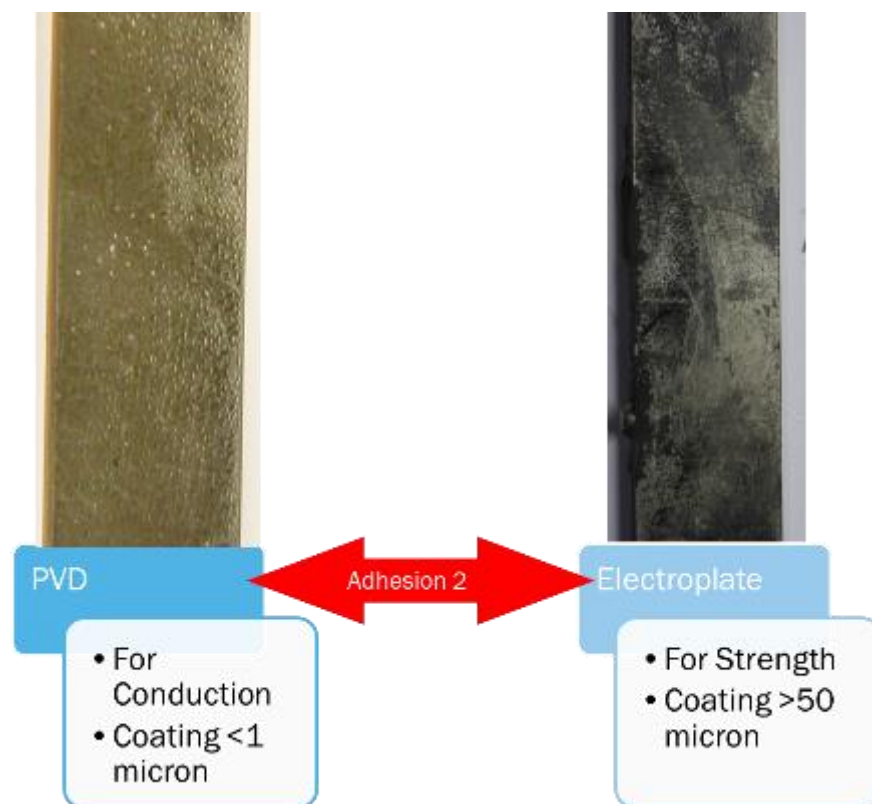
Figure 34 Description of Interface 2

The formation of percolating polymer formations was determined by removing the electroplated film as shown in Figure 34, on the left is the surface of the Ni film, and on the right is the surface of the sputtered coated CE. When comparing it to Figure 35 the main difference is that for the CPP process the PVD coating adheres to the e-plate as advent by the dull appearance on the bottom of the surface and the bare CE surface now visible. While again in Figure 34 with the PCP process the Ni e-plate is lustrous and clean and the bare surface is not visible. This indicates that in the PCP process the Ni e-plated is attracted to the Ni PVD coating during electroplating but does not from bonds with the coating and relies like in the CPP process.

Ultimately, the formation of the metallic bonds is inhibited through the PVD layer

Figure 36 Peeled Ni film from tested and fractured specimen created with the PCP process. Left Ni E-plate film surface, Right PVD Cyanate ester Surface

Figure 35 Two test specimen created with the CPP process. Left PVD coated cyanate ester surface, Right Ni Plated specimen with film peeled to side.

becoming corroded and polymer layers forming over nickel physically blocking bonding. This percolation occurs normally in CE221, but only interferences with the PCP process. This due to the percolation occurring when the PVD coating is highly susceptible to contamination.

3.3 Formation Layers Description

Building on the work of Bray's project, in this work it was discovered that due to intrinsic material properties and the vacuum processes used, uncured CE resin in printed parts percolates monomer through two surfaces, the as printed CE surface and the PVD coating. The resin percolation through the surface is causing a BLC formation and is intrinsic to the material, while the percolation through the PVD coating is called an SLG formation and primarily caused by the vacuum chamber and intensified by the BLC formation. The BLC formation leads to failure that primarily causes delamination as shown in Figure 36, while SLG layers block the electroplate film from forming bonds with the PVD as shown in Figure 37. These formation layers always occur after a thermal cure on the CE part where it then becomes permanent. Only SLG formation can be inhibited prior with either acetone or denatured alcohol, but these chemicals damage the base polymer and removal of these layer also diminishes the strength of the base polymer substantially.

To quantify and qualify the formation of the BLC and SLG formations, surface roughness

Figure 37 BLC caused failure example.
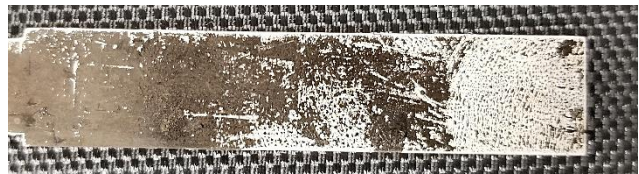
Figure 38 SLG caused failure example.

scans were taken using the laser scanning microscope of different test samples cleaned in various ways and with different cleaners. Within this section all surfaces were cleaned with the manufactures recommend process. Moving forward, after observation of the BLC and SLG formations and the qualitative effects of decreased adhesion between the PVD strike and the e-plated layer, work progressed to determine if a solvent cleaning process prior to PVD could prevent the egress of the uncured monomer through the photo-cured surface, thus mitigating the BLC and SLG formation and allowing the e-plated film to strongly adhere to the strike through

metallic bonds. The methods and the results of this experiment are described further on but can be summarized as inhibiting of the SLG formation and minimization of the BLC formation are detrimental to the sandwich composite overall.

3.3.1 Bake Layer Coalescence (BLC) Formation

The process is in which the part becomes polished or smoothed in an additive manner causing the surface roughness decreases on the micro and nanoscale. This is called a *"Bake Layer Coalescence"* or BLC-formation. It is caused when the mobile monomer migrates through the photo-cured polymer surface primarily during the thermal curing process This formation is intrinsic to any printed CE part goes through the thermal curing process and can only be mitigated and never fully removed.

As shown here in Figure 38 bellow, the heat map for the height of the surfaces is drastically changed through the curing process. As the printed surface is set in place through the UV cure during printing, it is necessary that this layer forms due to the egress or transport of uncured monomer from the interior of the part through thermally curing surface to the layer. Here after the surface typically takes on a smooth texture with high specular reflection without any intervention. The overall effect here is one of surface smoothing and "additive polishing" and is intrinsic to the Carbon CE material.

BLC layering additivity fills in micro/mini-macro and intrinsic defects. In Figure 38 , we show a microscope image and height map for an uncured and cured part that were cleaned with a paper towel and no cleaner. Observing the height heat maps, the top image (pre curing) indicates that there are distinct height differences and the presence of deep fissures with high ranges in between them. Observing the bottom image of Figure 38 the fissures become filled in

and smoothed over where unwashed resin cures and levels the surface parts by filling in surface geography and details that contribute to roughness.

The effects of the BLC layer are both beneficial and detrimental. One beneficial aspect of a BLC layer forming is the reduction or elimination of microscale and macroscale defects as seen in Figure 38 and later in Figure 46. The additive process will fill in pores, defects, and surfaces
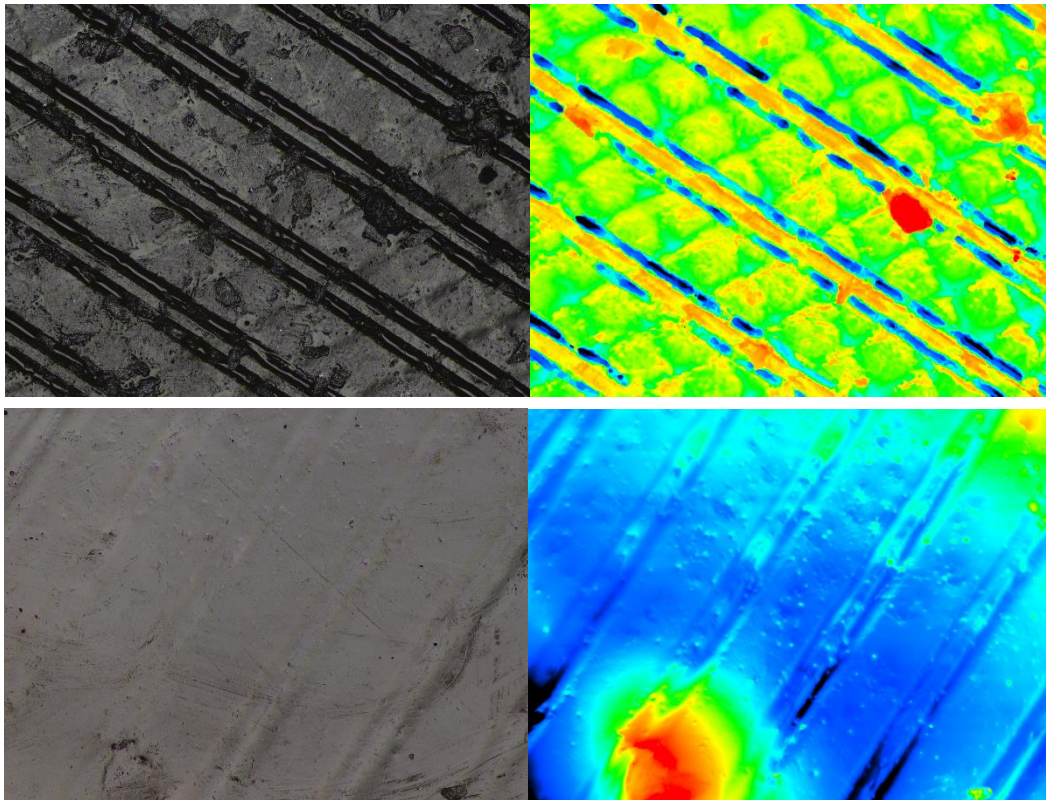
Figure 39 Example of a BLC Layer Formation, Above the Optical and Height Map of an uncured surface, Bellow the same part after curing.

leaving behind a surface that has been measured to have less than single micron roughness. Further, through surface profile scans it is shown that roughness on the order of 100 nm is drastically decreased from the formation of the BLC level. It is noted that roughness decreases on these scales should have detrimental effects to adhesion, and therefore the increase in adhesion observed here and in Bray is anomalous until the egress and intermixing of the polymer with the PVD is discovered in the form of SLG formations.

3.3.2 Surfactant Layer Generation (SLG) Formation

The second process that initiates during the vacuum chamber process and intensifies during curing, where the mobile monomer not only migrates through the photo-cured polymer surface of the part but also percolates through the PVD coating and settles over the PVD coating encasing and becoming permanent once thermal cured. This is called "Surfactant Layer Generation" or SLG formation. Once cured the layer cannot be removed through etching or sanding without damaging the PVD strike due to the adhesion characteristics. Subsequently the SLG formation is why Bray found the PCP process to yield the strongest results as the polymer layer would cover the PVD and lock it to the surface. Though it is also the main reason Interface 2 is drastically weakened too.

The generation of the SLG formation is shown in Figure 39. The top images are the surface of uncured PVD coated CE, and the bottom is the same specimen surface post thermal cure. In the top image the PVD strike is a consistent color and the striations the printing process caused, and the sanding process are visible and not filled in. In the lower image the striations are filled with the SLG formation which appears as white in the image. The SLG formation that forms over the PVD layer blocks the electroplating film from forming metallic bonds leading to failures

like in Figure 37. This removes the primary mechanic of the adhesion strength of Interface 2. Resulting in the secondary mechanism of mechanical interlocking from surface roughness the only factor in Interface 2's strength.
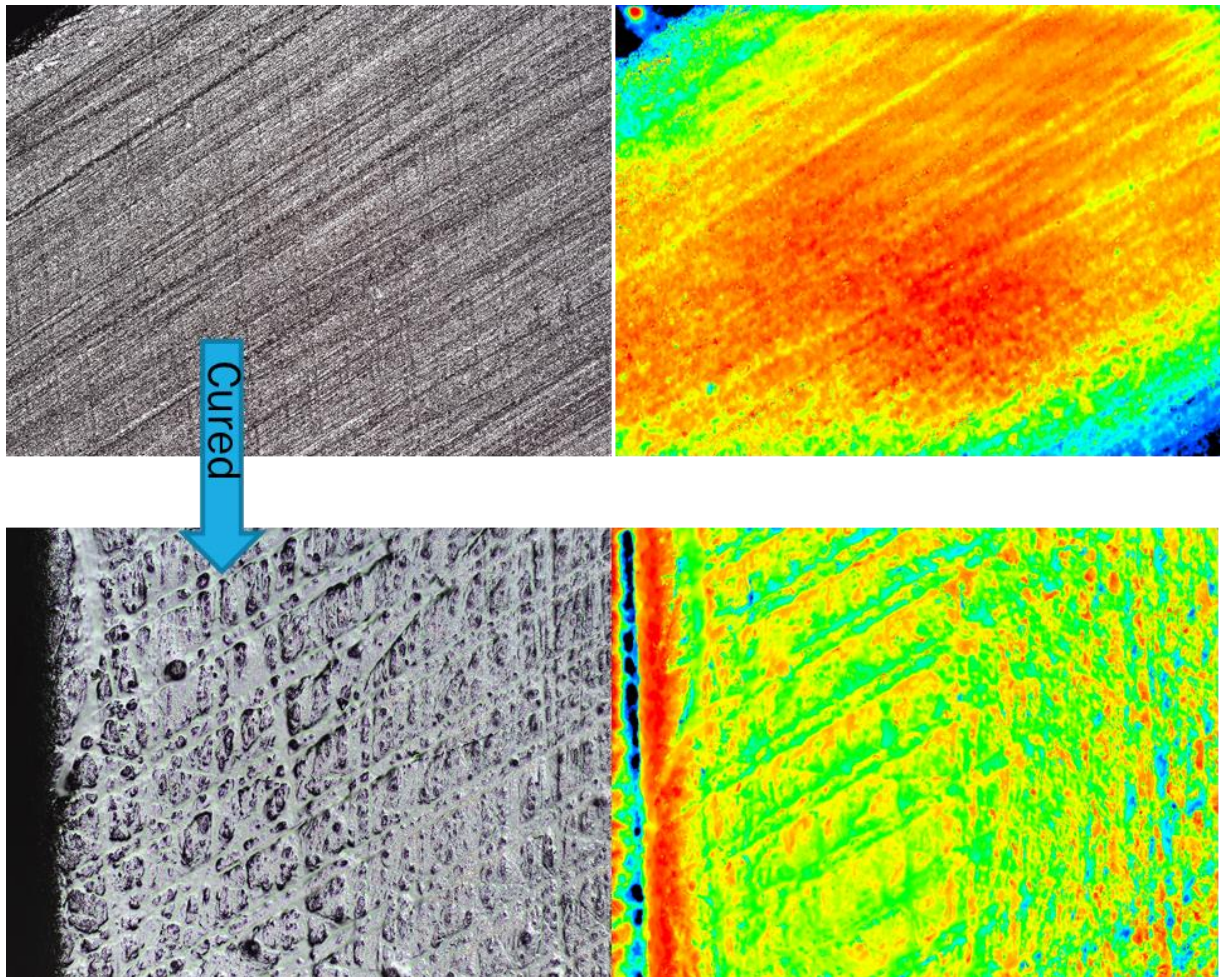
Figure 40 Example of a SLG Layer Formation, Above the Optical and Height Map of an uncured pat, Bellow the same part after curing.

The SLG formation is caused by the vacuum chamber used in the PVD coating process where low pressure vacuum environment outgasses the CE and draws out uncured resin components. To determine that the vacuum process is what draws the monomer through the PVD film, two sets of sputtered specimens were left exposed to vacuum after sputtering. One set had the BLC/SLG formation neutralized prior to sputtering via aggressive solvent treatment Figure 42. The other had no neutralization done Figure 43 both images were taken two weeks after the sputtering process. As seen the neutralized surface the coating looks metallic, similar to the target material of Ni. While the surface not neutralized looks tarnished and is obviously corroded, appearing drastically different from the other samples and the Ni target metal. In Figure 44 tarnishing becomes exasperated once the thermal curing of the resin is completed as shown the entire Ni layer surface has blackened likely has corroded.

Figure 41 Example of PVD coat on uncured BLC/SLG neutralized cyanate ester

Figure 42 Tarnished nickel coated uncured cyanate ester, left under vacuum for 24 hours.

Figure 43 Corroded Nickel PVD surface after thermal cure.

To further test this hypothesis, an uncured sample was placed into the vacuum chamber for 24 hours and subsequently scanned using FTIR analysis. FTIR analysis reveals that some organic material has percolated through the PVD coating, as evident by the polymeric peaks present on the FTIR scan. Optical inspection of the part also demonstrates discoloration and clear adulteration of the PVD layer chemically and morphologically It is evident here that the SLG formation not only compromises the clean interface of the PVD strike, thus drastically reducing adhesion to the e-plate, but also causes corrosion which prevents metallic bonding and increases resistivity of the strike.

The SLG formation becomes intensified with the BLC formation during thermal curing. As the BLC process alters the interface surface of the CE and PVD coating, it is observed through microscopy in Figure 43 that the mobility of the surface creates microscopic holes in the PVD strike. The SLG formation is therefore supplied with more mobile monomer if the underlying part undergoes surface reconstruction during curing. In addition, the combination of monomer and thermal energy during curing are hypothesized to cause increase corrosion of the PVD, further decreasing the possibility of mechanical bonds forming between the PVD strike and the e-plated Ni.
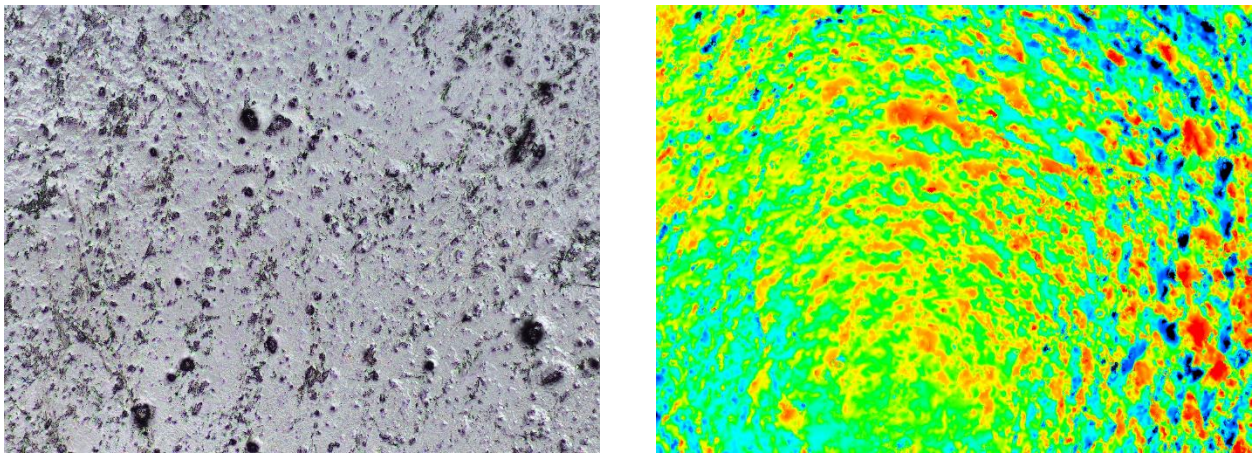
Figure 45 Laser Optical image (left) Surface scan height map (right), of cured cyanate ester with strike layer applied using the PCP process black holes aree actually higher than surface due to monomer percolating through these points.

3.4   Formation Layer Mitigation

BLC-formations are observed on all parts printed with CE and not neutralized, but the intensity is dependent on two things: <u>Time</u> and <u>Cleaning</u>.

3.4.1   Time

The amount of time before the thermal cure is applied where parts cured within the hour as seen when comparing surfaces under optical laser scan microscope. The uncured surface in Figure 44 shows a large degree of surface roughness while the cured 2 hours after printing surface, Figure 45, have intense BLC layer formations and roughness filled in. The surface cured 2 weeks after printing Figure 46 maintains some roughness similar too Figure 44. But large amounts of surface roughness are still filled in. This means the time a CE part waits until the final thermal curing application is applied the affect the BLC and SLG formation, and increases the surface roughness of the PVD strike, that increases the adhesion mechanic of interface 2.
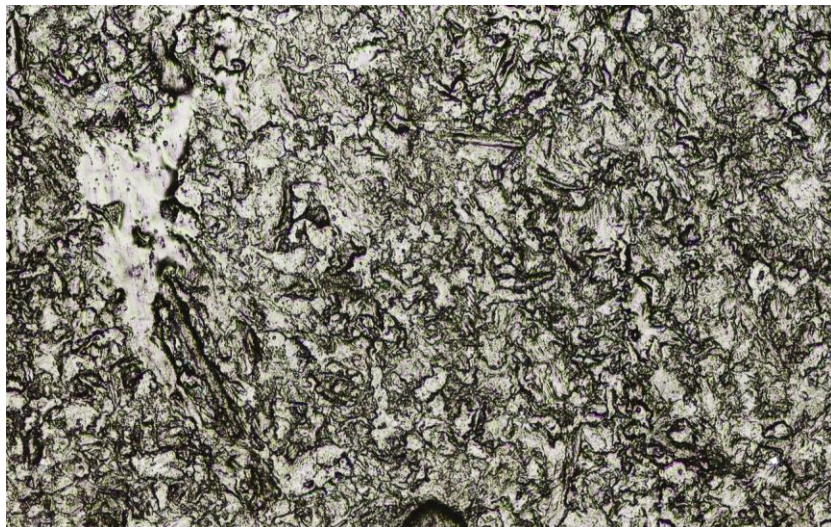
Figure 46 Uncured cyanate ester wiped with cleaner surface, illustrating surface roughness.
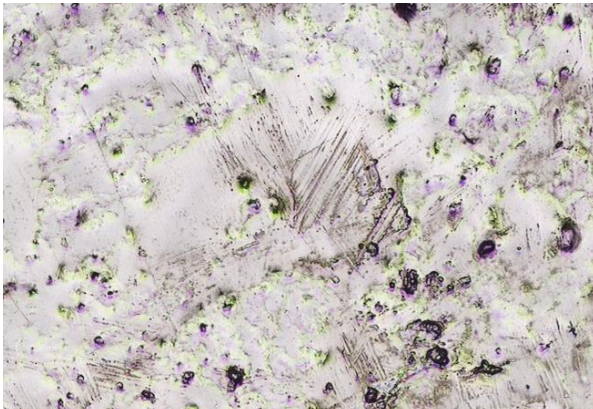
Figure 47 Surface of cyanate ester wiped with cleaner post cure, example of BLC forming on surface cured within 2 hours of printing.

Figure 48 Surface of cyanate ester wiped with cleaner post cure, example of BLC forming on surface cured with in two weeks of printing.

This is why the initial PCP process results were so sporadic. When a longer lead time was used during sample production involving the PCP process the CE part could be successfully plated due to the increased surface roughness. While samples produced in a timely manner more consistent with manufacturing would not and create SLG formations. Testing described later in this paper attempted to isolate the main time dependent factors with little success. As of now it is assumed to be due to natural out gassing over time and possible environmental exposures such as ambient temperatures and moisture in the air.

3.4.2 Cleaning

The second factor the BLC and SLG formation intensity is dependent on is the cleaning methods employed. No method of non-invasive cleaning can inhibit the formations, but the best results require the combination of wiping the surface with cleaner prior to washing the surface with the cleaner. The BLC formation diminishing effects of cleaning methods is shown in Figure 52 through Figure 48. Shown are optical laser scans of the surface of CE, uncured surfaces are on the left, and cured surfaces are on the right. Microscale pores are not present that were not in giving the surface more roughness. All surfaces show BLC formations to varying degree during the transition of curing. The most intense BLC formation is Figure 52 where no wiping was used, while the most diminished BLC formations occurs in in Figure 48 when the combination of wiping and an orbital stage was used. As mentioned, prior, the formation of BLC contribute to the formation of the SLG formation, affected by cleaning methods as well
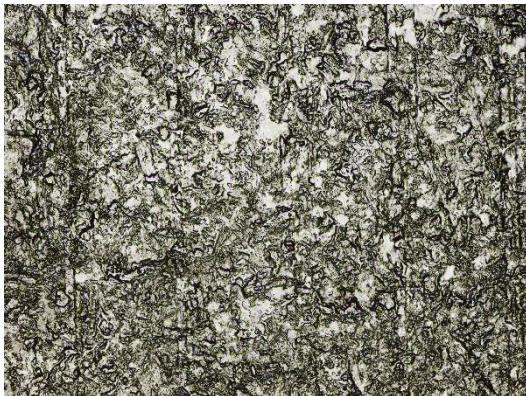
Figure 49 C.E Surface of uncured IPA PG orbital stage and wipe
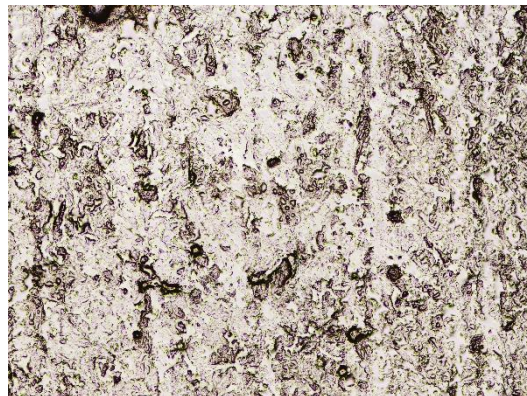
Figure 50 C.E Surface cured IPA PG orbital stage and wiped.

Figure 52 C.E Surface uncured IPA PG wipe

Figure 53 C.E Surface cured IPA PG wipe
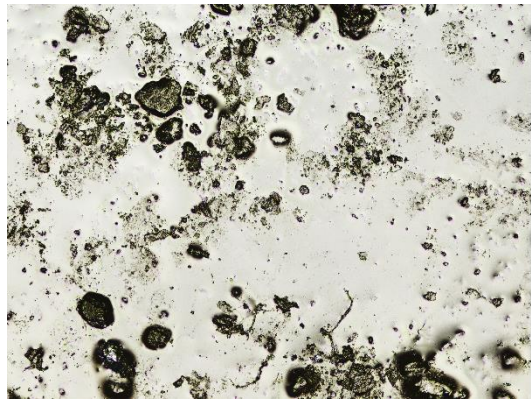
Figure 54 C.E Surface IPA PG orbital stage
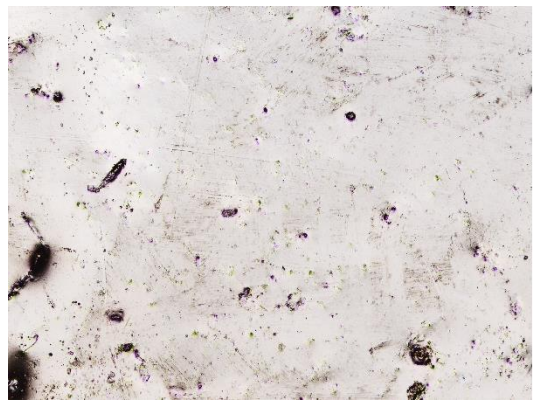
Figure 51 C.E Surface cured IPA PG orbital stage

BLC formations are hypothesized to form from two sources prior to thermal curing "agitation" and uncleaned resin. Increasing the temperature of the part causes the expansion of any uncured monomer, as well as a decrease in effective "viscosity", which allows the monomer mobility to and through the top photo-cured surface. Uncleaned resin that clings to the surface from the part printing process also lacks stability due to a lack of photocuring. When the part is heated during curing the uncleaned resin is able to translate to minimize surface energy and smooth. The results are a drastically altered surface that also affects the interface of the PVD coating to the Polymer. BLC layers are believed to be the cause of the diminished adhesion strength of the PVD coating to the CE surfaces. As the drastic altering disrupts the interface 1 adhesions and PVD film.

3.5 Thermal Curing Effects on the PVD Coating

During the project commonly, it was observed that the previously metallic Ni coating picture in Figure 53 as the two specimens on the right, would discolor to a black or dull orange grey as shown as the 2 left most specimens in Figure 53, The black and darkened appearance is believed to be caused by the corrosion of the Ni with has a darker appearance. While the still metallic looking Ni layer appears tarnished. This blackening occurred throughout all initial samples made for testing and seems to be a one of the causes that leads to diminished strength effects.

Figure 55 Pre and Post Cure transition, Left to Right (Post, Post, Pre, Pre)

Upon fractography of the fractured parts that were tested a peculiar occurrence was observed, where the bottom surface of the Ni e-plated film has looks like a normal Ni metal surface and even more lustrous than the top surface of the film. The blackening of the PVD layer surface commonly on occurred on parts cleaned with IPA, IPA + PG, and occasionally on parts cleaned with acetone, but not parts cleaned with denatured alcohol. The bottom of the Ni-plated film would never pick up blackened color entirely only occasionally in samples cleaned with an IPA or D.A. mixture. Excluding these occasional blemishes, the bottom of all electroplated films I.E., the film the generated from the PVD surface were highly lustrous compared to the top surface of the Ni.

With parts Cleaned in Acetone being the clearest and DA being the most tarnished but still bright and IPA being the dullest.

More specifically on the film quality and texture that each cleaning process produced, all parts plated using the PCP process produced a top surface plate that was dull and matte. When compared the top surface to the bottom surface layer of the Ni plate film the bottom was always much brighter. Films generated on specimens cleaned would always pick up the surface morphology associated with that surface. If surface feature, fissures, or crazing were present the film would generate the same texture, that the PVD layer have. Once the film was lifted from the PVD layer, the PVD would be the same color blacked or metallic tarnished color it was prior and be able to be electroplated to again in certain instances. Very rare to see bare CE after the plate was removed without the aid of a microscope, meaning the PVD removed with the Ni-plated film was very minute. If the PVD is adequately adhered to the part the bottom layer of the film should be blackened as well, or the bare ester should be easier to see.

Assuming that the PVD layer was turned black, corroded during the formations of the SLG & BLC layers, the entire coating can be assumed black. This is proved by polishing a PVD coated ad cure part to the orange core in Figure 54. If there was a hidden lustrous Ni layer formed in a sandwich of corroded PVD it would be observable after a light polish which was not the case. Instead, once the Ni film was removed from the part, the bottom of the Ni film would be mostly lustrous in appearance, and there were only occasionally blacken and dull orange-grey spots on the bottom and a blemished appearance on surface of the PVD.

The fact that the Ni films pick up the characteristic of the surface the film if generated on means that during electroplating the film is attracted to the PVD layer, but because the film cannot remove any of the PVD from the CE surface means no bond metallic bonds formed. Indicated by the corroded PVD surface with a portion of the sanded to display the base material Figure 54. This show that the base substrates color is still orange, thus if the PVD coat adhered to the e-plated film the orange CE would be visible. It was assumed that the darken spots were areas where adhesion to the Ni plat and PVD were strong, and spots where the removal of the Ni film accompanied by CE were the strongest.

Figure 56 Corroded surface PVD with polished section showing bare cyanate ester.

The likely cause of the blackening and the PVD becoming covered is the BLC and SLG formation layers, respectively. The BLC formation alters the surface geography of the CE PVD interface layer disrupting and altering the adhered PVD coating and presumably allowing for the SLG formation the form easier thought the disrupted cracks. The SLG formation will permeate through the covering the coating and presumably corroding the Ni as well.

These two-effects feed into each other as well, once the PVD layer becomes blocked by the cured/uncured CE layer or "" the adhesion of the Electroplate to the CE part is dependent on surface friction that stems from the surface roughness. Since the CE part will additively polish the

surfaces that have not been inhibited, the surface roughness drastically reduces. This diminishes the main factor in the adhesion of the electroplate to the PVD layer, friction. The only way to prevent the SLG Layer from forming and cause the part to become Becca-dd in is through inhibiting the surface during surface prep and prior to curing.

This means that determining the correct surface prep techniques, which included chemical used and methods of cleaning, was paramount for the project success. This needed to take place prior to curing. As most post cure surface prep would damage the PVD layer when trying to remove the SLG layer, and once a surfaced became BLC layered and cured it was permanent. The ideal techniques in being inhibiting the surfaces of printed parts from generating a SLG layer and thoroughly cleaning parts to prevent BLC Formation from occurring.

Chapter 4 Results

In this chapter we discuss the results of the experiments conducted throughout this project. Observations, outline recommendations for future works, and next steps to move forward with reinforcement process will be reviewed. Including the processes necessary to metallic reinforced CE through the PCP process. Methods of treatment prior to thermal curing to attempt to reduce or eliminate the egress of uncured monomer through the PVD layer through the BLC and SLG formations. An overview of recommendations to alter the process of metallic reinforcement to provide more evenly distributed adhesion strength to the two interface surfaces.

4.1 Wiping study and Curing Orientation

The SLG formation and subsequently BLC Formation was believed to be caused by two factors: Cleaning methods and the curing orientation. Though the results of the curing orientation are inconclusive due to the discovery the time spent till curing occurred effected SLG migration more. The cleaning methods do effect mitigation overall. Specifically, the combination of wiping parts and the use of an agitation cleaning method such as ultrasonic baths or orbital stages. The can be seen in priors in Figure 48 through Figure 52 through Solvents such as IPA, IPA+PG, can prevent some BLC formation and occasionally prevent the SLG formation from occurring but the results are often inconsistent and only prevented effects either on the top or bed surface zone which led to the previously stated assumptions.

4.2 Chemicals and UV effect on Mitigation

4.2.1 UV Light

During testing exposure of UV light was used to see if a light overcuring of the photo polymer could reduce the SLG formation and strike corrosion. The results indicated that there were more prevailing factors to mitigating the SLG formation as the control group with no exposure to UV light had a mitigated SLG formation Figure 58. Though all specimens were able to be Electroplated to some degree the corrosion of the strike still occurred Figure 59 the addition of the more curing to the surface also introduced fracture seen in Figure 60, this occurred the surface of most parts exposed to longer than film. Thus, light over exposure to UV light does not aid in reducing the corrosion, not mitigating the SLG formation. The control specimens were able to have the SLG formation mediated due to two things. One, this being the first time wiping of the surface was used on the specimens. This was added to remove residual resin so it would not absorb the UV light meant for the surface polymer. Two, the amount of time the experiments took for the specimens to be sputtered and cured. This allowed the CE to out gas mildly thus reducing the BLC and SLG formations
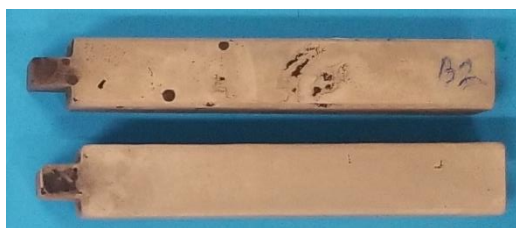
Figure 57 Control Group for UV exposure experiment

Figure 59 UV exposure specimen with mild fractured cause from overs exposure

Figure 58 UV exposure test group demonstrating an corroded Strike surface and SLG formation blocking.

4.2.2 Acetone

Acetone was originally used as a bath for the specimens to remove residual resin prior to PVD. Upon curing it was realized that acetone baths caused intense crazing of the top surface zone shown in Figure 58 enhanced in Figure 59.

Figure 61 Example of Bed layer artifact Crazing

Figure 60 Crazing of Bed layer artifacts under microscope.

The cleaning study found wiping made crazing take on a milder response on the bed surface zone and little to no effect on the top and voxel surface zone. If any form of agitation was used when cleaning parts, Intense crazing and PVD coating corrosion occurred as shown in Figure 59. Though acetone also has the ability to inhibit the SLG formation and removes all forms of BLC prior to curing and neutralizes the SLG from forming after curing. Though it was a mistake Acetone proved very useful and was even incorporated into the final PCP process

Figure 62 PCP process Acetone cleaning specimens, Surface zones various

Bellow in an example of the transition that occurs when cleaning acetone. In Figure 61 and Figure 62 parts become crazed but exhibit ideal PVD strike quality after sputtering but corroded intensely after curing.

Figure 66 Example of Acetone bath exposure's effects on the bed surface zone throughout the PCP process, Top to bottom: Uncured, PVD, PVD-Cured

Figure 65 Example of Acetone bath exposure's effects on the Top surface zone throughout the PCP process, Top to bottom: Uncured, PVD, PVD-Cured

4.2.3 Denatured Alcohol

Denatured Alcohol or D.A has a similar effect to acetone where prolonged exposure can encase crazing of the parts, Figure 63 and shown enhanced in Figure 64. D.A also does not reliably remove the SLG layer reliably as seen in the gradient study done in Figure 65. By the time enough exposure to the D.A has occurred to diminish the SLG formation, the DA will craze and embrittle the parts.
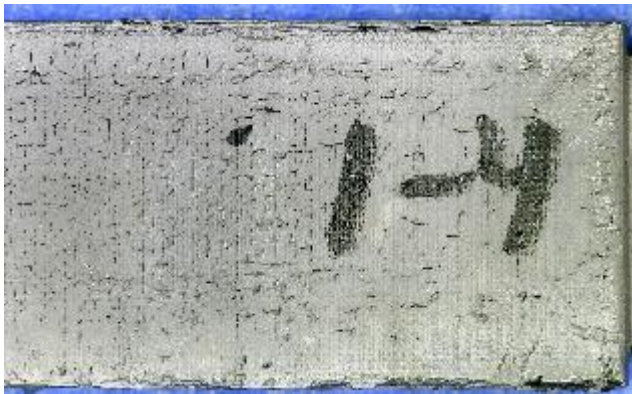
Figure 67 Example of the surface of a D.A cleaned specimen exhibiting chemical etching

Figure 68 Microscope image of the D.A etched surface

Figure 69 Gradient study examples of DA.

4.2.4 IPA 99.9% + Propylene Glycol 50/50

The IPA+ PG mixture does not provide any consistent inhibiting of the SLG formation and very limitedly prevents BLC formation as shown in Figure 52 through Figure 48 prior.

4.3 Plating and the PCP Process

In order to use the process laid out by Bray [6], the adequate surface prep procedure needed to be developed. This is due to the previously mentioned SLG/BLC formations preventing the adhesion of the Ni e-plate to the PVD strike. This experimental plating process followed the steps mentioned in the Table 1 with the addition of a secondary wiping process. The additional step involved gently wiping the PVD strike surface after full application. The wipe would test if the strike layer were removable and used either IPA or Acetone depending on if the surface were the top surface or bed surface, respectively. This was because Acetone would craze the top surface but not the bed layer. Follow the steps mentioned in *Table 2 Multi-Current Plating Process*. This additional process successfully diminished the BLC and SLG formations allowing plating adheres through surface interlocking but did not prevent the corrosion of the PVD strike inhibiting the stronger chemical bonding I.E., any metallic bonds from forming at interface 2.

4.3.1 Material Test Results

In the following we present the results of the three-point bend testing on the control samples, cast samples, and samples with an applied metallic coating. Table 3 contains the processed data and Figure 65 shows typical stress-strain curves for the testing. Here, the manufacturer cited a flexural strength of 125 MPa, and the printed control group cleaned with the manufacturer specified process demonstrated an average flexural strength of 152 MPa with a standard deviation of 7.7MPa. Samples created through the casting method demonstrated a lower maximum flexural

strength, only achieving an average of 95.8 MPa with a larger standard deviation of 29 MPa. The plated group exhibited a maximum flexural strength of 112 MPa at fracture, with a standard deviation of 10 MPa. As shown in the stress-strain curves of Figure 65, while the failure stress is higher for the non-plated controls, the plated parts demonstrated a flexural stiffness more than twice that of the non-plated controls.
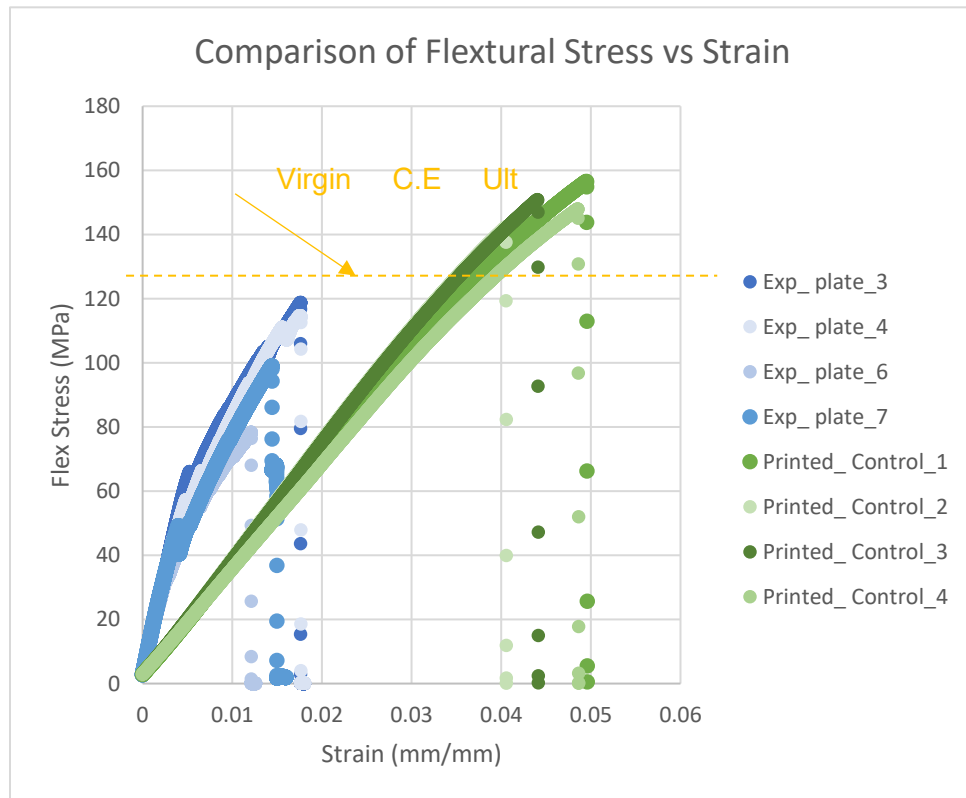

Figure 70 Stress vs Strain Graph of Plated and controls

Table 3 Three Point Bend Test data for CE

Process	Max Flexural Strength (MPa)	Error (+/- MPa)
Virgin CE	125 [23]	~
Printed controls	152	7.7
Experimental Plating Process	112	10.1

Cast Controls	95.8	29.0

Using the Equation 5, listed below, the bending moment required to cause a theoretical failure in EPP test groups was investigated. It was determined that failure would occur in the Ni film prior to the CE at a given metal film thickness between 50-70 microns. The stress this occurred at was then calculated using Equation 2 to be between 30 to 47 MPa.

Equation 5

$$\sigma_j = E_j * \frac{Mt}{\sum[E_i I_i]}$$

- σ_j: Stress developed in Material J.
- E: Youngs Mod. of Material
- M: Moment applied
- T: distance from Neutral Axis
- I: area moment

After testing, Printed controls, Experimental Plated Process (EPP), Cast Control tests samples the results indicated that the 3D printed control samples had the largest ultimate strength for all tests groups will all the results tabulated in *Table 3*. Even compared the pure CE material properties, 3D printed CE controls had a larger flexural strength than all other groups. The plated group demonstrated increased stiffness but also decreased stress at rupture, due the composite nature of the sample.

The printed controls have a higher flexural stress due to the benefits the BLC formation provided to the part as it fills small scale defects on the surface and intrinsic defects caused by printing Figure 38 and Figure 67 respectively. This increases the printed CE flexural strength by removing structural defects. Thus, the inclusion of the BLC layer provides a labor free method of finely polishing parts and strengthening them, though at the cost of inhibiting Interface 2.

Although it may seem counter intuitive that the EPP test group had an ultimate flexural

Top layer Artifacts
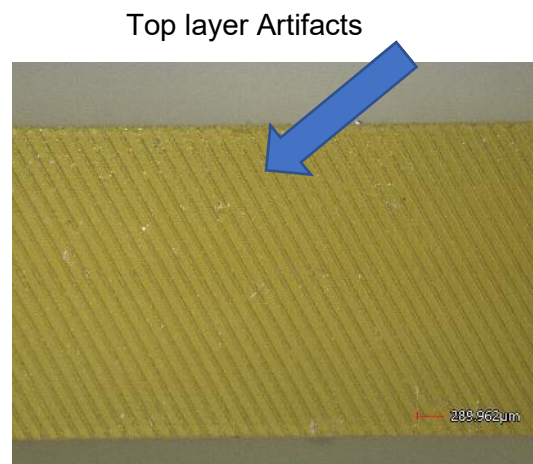
Figure 72 Top Surface Layer Artifacts

stress lower than the printed controls, the composite beam theory hand calculations demonstrate that this is to be expected. When the composite beam is loaded, the much greater stiffness of the Ni layer dominates the mechanical response of the beam. As the layer is very thin compared to the bulk CE cross-section, the load for failure of the coating is lower than that of the CE, although the respective strain at a given load is much larger for CE. When the Ni layer fails, the inner CE part takes the load rapidly and failure is initiated in a different way than in the case of non-coated controls. *Table 3* . In Figure 66 the EPP shown in blue can be seen to exhibit load drops, common in composite materials when one of the materials begins to yield or fail [24]. This causes the sample to weaken, allowing the sample to be displaced at lower forces indicating permanent damage and possible failures are occurring at much lower stresses more near to 60MPa. This is

consistent with the hand model calculations that determine failure would occur near a stress of 47MPa. This validates that the Ni incasement is failing and exposing the substrate material to the environment which is not a desired outcome. Making true failure of the part mores consistent with 60MP, when based of hand models, but still weaker when compared to the control group.

While the Cast CE had the weakest flexural strength overall. The cast CE was also observed to be a different color that the cured CE and more similar to uncured CE. As no photocuring was supplied to the CE the cause of failure is due to under activation of the polymerization process through no photo cure. Upon realization the polymer was disposed of due to the carcinogenic nature.

Chapter 5 Conclusions

In summary, this work presents findings on the effects of processing parameters and order in metallized 3D printed CE parts. It is determined that previous work to maximize the adhesion of the PVD strike layer also causes detrimental coupled effects to the adhesion of a thick electroplated Ni layer to the strike. The effects of the BLC and SLG formations are beneficial to strengthening the adhesion of the PVD strike to the CE base but ultimately damage the Ni strike coating. through corrosion and encasement, thus preventing metallic bonding between the strike and the e-plated layer. As the bulk of the strength, or flexural stiffness, of the sandwich composite comes from the Ni plating the PCP process fails to be effective with this combination of materials. Further, delamination failures are not acceptable for the end use case as detailed by the sponsor, requiring the author to investigate alternative process methods.

One path of investigation was if solvent cleaning could prevent the egress and corrosion of the PVD strike through solvent cleaning of the CE substrate surfaces prior to metallization. Developing processes into mitigating the BLC and SLG formations proved ultimately detrimental to the base polymer overall the manufacturer's method of cleaning does little to negate the formations, and solvents such as Acetone and DA can inhibit the formations but at the cost of damaging the base polymer through embrittlement and crazing. With no solvents shown to prevent the main issue of corrosion from occurring without damaging the base polymer. The damaging effects of BLC/SLG removal outweigh the beneficial additive polishing effect the BLC formation, as parts that exhibit this have a strength 25% stronger in flexural strength than the virgin cast CE.

In conclusion, an effective metallization process for sandwich composites involving multi-step curing resins must allow the resin to cure without damage to metal reinforcement layer. The

PCP process does highlight that mechanical interlocking of PVD sputtered films can be increased by fully polymerizing or curing parts after the application of the coating. special considerations must be taken to ensure the coating does not become contaminated through the application or curing process. In leu of this when a CPP process is used to make parts paramount is the inclusion of surface roughness prior to sputtering. In the case of CE traditional adhesion techniques do not work as CE is extremely resistant to etchants and acids. Which means alternate avenues that increase surface roughness or surface area will result in stronger sandwich composite. composites.

The following are recommendations for methods that can achieve more ideal results and a recommended process for future works.

There are a total of four methods that can be used to successfully metalize a part for future works, mainly taking advantage of the material properties, mitigating the out gassing that occurs during the vacuum chamber process of sputtering. Balancing the two interface strengths is more important overall then just maximizing one interface.
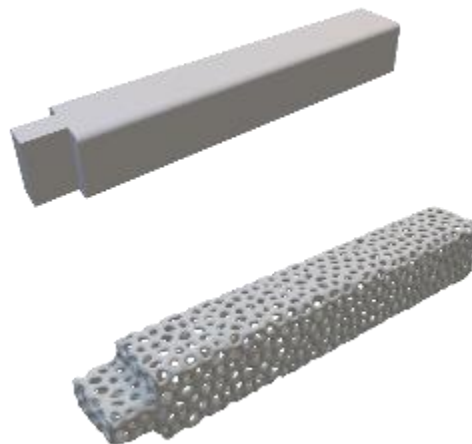
Figure 73 Base shape converted to a lattice shape.

1. Increase the sandwich part through material means as opposed to adhesion mechanics.

   a. The total amount of Ni plating used can be increase through lattice base shapes.

b. Lattice shapes increase the surface area of the base part. Figure 68.

c. Transitions the stress failure mode to material failure rather than a delamination.

The addition of more reinforcement material in a composite is known to increase the composite material's strength. Lattices are an easy way of doing this through the addition of increased surface area. As the amount of Ni that can be plated is proportional to the amount of surface area a part has, the increase in surface area increases the Ni volume fraction. A larger volume fraction will also lead to more dominating mechanical encasement by the Ni as compared to the samples in this study.

Figure 75 CPP process Specimen sanded prior to PVD coating.

2. Take advantage of BLC formation by using the CPP process and introduce roughness through sanding or dry ice blasting.

a. Printed parts with a BLC layer are 25% stronger than those without.

b. Introducing roughness prior to sputtering, but after curing, keeps all the benefits of the processes.

c. Removes the damage caused by the vacuum chamber and allows the formation of metallic bonds.

Bypassing the detrimental effects of the SLG formation and keeping the beneficial effects of the BLC formation can be done by using the CPP process. The material is stronger, and only needs the addition of surface roughness to increase the adhesion mechanic. When done prior to sputtering, dry ice blasting or sanding can increase the surface roughness without contaminating the PVD film.

3. Use a material that can be post cured thermally but does not outgas or percolate monomers or solvent vapors that can corrode the PVD strike layer or exhibit a drastic change to surface morphology.
   a. Thermal curing is effective in a PCP process as UV-light is blocked by the strike.
   b. Outgassing that corrodes the strike must be prime consideration.
   c. Adheres to established PVD adhesion mechanics.

It is possible for the PCP process to be used so long as the effects of the PVD film are considered. One big issue that went unnoticed in this project for a long time was hat the PVD was becoming corroded after curing, inhibiting the e-plate film from bonding. The polymer must reach a final cured state without damage to the film through thermal curing. No UV curing can be done after the sputtered film is applied as the bulk of metals do not allow transmission of UV light through the surface but do conduct heat.

4. Use SLA sintering 3D printed polymers.
   a. Shown to be strengthened.
   b. Higher polymer activation density reduced outgassing.

SLA sintered polymers have been shown to exhibit lower outgassing during the vacuum process allowing for less contamination to occur in the PVD sputtered film. The higher polymer activation

density that occurs in laser sintered parts causes this, as less residual monomer is left in the base

material.

The ideal process to metal encases a multi-step vat photopolymerized part is as follows:

1. Print and clean CE part with manufacturer's method.

2. Cure part within an hour of completing print.

3. After curing, introduce roughness through sanding or dry ice blasting; a roughness of 320-400 grit is acceptable.

4. Wash part again with manufacturer's method to remove any dust.

5. Sputter substrate with PVD strike layer.

6. Plate a low current density at first, then increase as needed when time goes on.

References

P. P. a. I. M. ". c. a. a. e. c. a. t. B. Navinsek.

1]

Nickel Institute, "Nickel Plating Handbook," Nickel Institute, 2014.

2]

Nickel Institute, "Nickel electroplating," Nickel Institute, [Online]. Available:

3] https://nickelinstitute.org/about-nickel/plating/. [Accessed 30 April 2021].

3D Sourced, "The Complete Digital Light Processing (DLP) 3D Printing Guide," 3D

4] Sourced, 19 September 2019. [Online]. Available: https://www.3dsourced.com/3d-printing-

technologies/digital-light-processing-dlp/. [Accessed 30 April 2021].

Carbon,   "Digital   Light   Synthesis™,"   Carbon,   [Online].   Available:

5] https://www.carbon3d.com/our-technology/. [Accessed 22 MArch 2021].

O. Bray, *Investigation of Vapor Deposited Conduction Seed Layer,* Jacksonville:

6] University of North Florida , 2020.

Standard Terminology for Additive Manufacturing, ISO/ASTM52900-15, 2015.

7]

C. W. Hull, "Apparatus for Production of Three-Dimensional Objects by

8] Stereolithography". USA Patent US4575330A, 08 August 1984.

R. J. Z. a. R. M. Castaneda, "Evaluation of Cyanate Ester Prepreg Material

9] Exposed to Uncontrolled Thermal Conditions During Storage," [Online], Available:

http://www.dtic.mil/docs/citations/ADA506883., Sep. 2009.

M. Hughes, SEMICORE Equipment, Inc., [Online]. Available: http://www.semicore.com/what-is-pvd-coating. [Accessed 27 November 2019].

[10]

J. W. Hutchinson, "Stresses and Failure Modes in Thin Films and Multilayers," Technical University of Denmark, Cambridge, MA, 1996.

[11]

S. J. Hearne, *Origins of Stress During Electrodeposition,* Albuquerque.

[12]

U. U. B. E. A. Yasin Kilinc, "Residual Stress Gradients in Electroplated Nickel Thin Films," *Microelectronic Engineering,* vol. 134, no. Febuary, pp. 60-67, 2015.

[13]

M. P. A. J. F. S. M. S. N. A. F. a. W. I. M. J. K. Luo, "Effects of Process Conditions on Properties of Electroplated Ni," *Journal of The Electrochemical Society,* vol. 10, pp. 155-161, 2006.

[14]

G. Richardson, "Measurement of Residual Stress in Electrodeposited Nickel Films (Theses)," Rochester Institute of Technology RIT Scholar Works, Rochester, 1999.

[15]

D. M. Mattox, "A Short History: Adhesion, Interface Formation, and Stress in PVD Coatings," *SVC ,* pp. 32-37, 2016.

[16]

C. V. Thompson, "Stress Evolution During Vomler-Weber Growth of Thin Flims," Dept. of Materials Science and Engineering, Massachusetts Institute of Technology, Cambridge.

[17]

Carbon, "CE 221-Carbon," Carbon, [Online]. Available: https://www.carbon3d.com/materials/ce-221/. [Accessed 19 April 2021].

[18]

A. International, *Standard Test Methods for Flexural Properties of Unreinforced and Reinforced Plastics and Electrical Insulating Materials,* ASTM International , 2017.

[19]

A. G. Melendez, Structural and Dielectric Properties of Molybdenum Doped Cobalt
20]   Ferrite, Material Science, 2016.

Standard Test Method for Core Shear Properties of Sandwich Constructions by
21]   *Beam Flexure, C393/C393M,* 2020.

D. Wells, "Metallic Laser Beam Powder Bed Fusion Process Qualification," in *1st*
22]   *ASTM Additive MAnufacturing Center of Excellence Workshop*, Auburn, 2019.

L. S. A. N. C. .. V. a. C. .. G. I. Mondragón, "Properties and Structure of Cyanate
23]   ester/Polysulfone/Organoclay Nanocomposites," *doi: 10.1016/j.polymer.2006.03.047.,* vol.
vol. 47, no. 10, p. 3401–3409, 2006.

A. Schrader, "Composites Jargon Explained – Load vs Displacement Control,"
24]   AutoDesk,   18   JANURAY   2017.   [Online].   Available:
https://blogs.autodesk.com/simulation/2017/01/18/composites_jargon_explained_-
_load_vs_displacement_control/. [Accessed 27 April 2021].

S. S. L.B Freund, "1.8.3 Tensile Stress due to island contiguity," in *Thin Materials:*
25]   *Stress, Defect Formation and Surface Evolution*, Cambridge, Cambridge University Press,
2004, pp. 68--72.

A. Kandelbauer, "11 - Cyanate Esters," in *Handbook of Thermoset Plastics (Third*
26]   *Edition)*, WIlliam Andrew, 2014, pp. 425-457.

Semicore,   [Online].   Available: Available:
27]   http://www.semicore.com/images/photos/diagram-sputtering-process.png..   [Accessed
April 2020].

Keyence   ,   "VHX-7000   Series,"   [Online].   Available:
28]   ttps://www.keyence.com/mykeyence/?ptn=001&gclid=CjwKCAjwvtX0BRAFEiwAGWJyZ

OaxdVxc2fpNwkyz_ZBVPVVzpZwrLI4aj21xVmfkVcIJl0CZo_KFHxoC6I0QAvD_BwE&k_c
lickid=4e8309e7-21a8-42e8-8ac3-440585927697&aw=google-kaenVH262102ee-br21a8-
42e8-8ac3-440585927697&aw=google-kae. [Accessed April 2020].

29]   ecourses, "Mechanics - Theory," [Online]. Available: http://www.ecourses.ou.edu/cgi-bin/ebook.cgi?topic=me&chap_sec=06.1&page=theory. [Accessed 29 April 2021].

30]   Z. . Tang, R. A. Black, J. M. Curran, J. A. Hunt, N. . Rhodes and D. . Williams, "Surface properties and biocompatibility of solvent-cast poly[ε-caprolactone] films," *Biomaterials,* vol. 25, no. 19, pp. 4741-4748, 2004.

31]   W. &. R. D. &. V. C. &. R. C. &. D. P. Decker, "Metallized-Polymer-Films-as-Replacement-for-Aluminum-Foil-in-Packaging-Applications.," 2004.